

doi:10.3799/dqkx.2017.042

内蒙古西乌旗南部晚古生代侵入岩年代学、 地球化学特征及地质意义

刘 敏¹, 赵洪涛¹, 张 达^{1*}, 熊光强², 狄永军¹

1. 中国地质大学地球科学与资源学院, 北京 100083

2. 江西省地质矿产勘查开发局物化探大队, 江西南昌 330002

摘要: 为探讨兴蒙造山带南蒙古陆块南缘晚古生代的构造演化, 对出露于西乌旗南部石英闪长岩、花岗闪长岩和黑云母花岗岩开展了详细的年代学、岩石地球化学及 Hf 同位素特征研究。结果表明: 石英闪长岩、花岗闪长岩和黑云母花岗岩分别形成于 330 ± 2 Ma、 274 ± 1 Ma 及 271 ± 1 Ma~ 282 ± 1 Ma。石英闪长岩属高镁闪长岩/安山岩类(HMA), 与俯冲洋壳板片上部地幔楔中地幔橄榄岩的熔融作用有关, 而花岗闪长岩及黑云母花岗岩的源区可能与新生地壳的部分熔融有关。结合区域成果, 推测西乌旗南部晚古生代侵入岩均形成于古亚洲洋向北侧南蒙古陆块持续俯冲的阶段, 早石炭世石英闪长岩属活动大陆边缘弧岩浆活动, 早二叠世花岗闪长岩和黑云母花岗岩则是俯冲过程中短暂弧后伸展阶段的产物。

关键词: 兴蒙造山带; 晚古生代; 弧岩浆; Hf 同位素; 俯冲; 地球化学; 地质年代学。

中图分类号: P581

文章编号: 1000-2383(2017)04-0527-22

收稿日期: 2016-06-15

Chronology, Geochemistry and Tectonic Implications of Late Palaeozoic Intrusions from South of Xiwuqi, Inner Mongolia

Liu Min¹, Zhao Hongtao¹, Zhang Da^{1*}, Xiong Guangqiang², Di Yongjun¹

1. School of Earth Sciences and Resources, China University of Geosciences, Beijing 100083, China

2. Geophysical and Geochemical Exploration Brigade, Jiangxi Bureau of Geology and Mineral Resources, Nanchang 330002, China

Abstract: In order to discuss the tectonic evolution of the Xing-Meng orogenic belt during the Late Palaeozoic, this study conducts a systematic study of the chronology, geochemical compositions and Hf isotopic characteristics of the quartz diorite, granodiorite and biotite granite from the south of Xiwuqi, which is situated at the southern margin of the southern Mongolian terrane. Zircon U-Pb dating indicates that the quartz diorite, granodiorite and biotite granite were emplaced at ca. 330 ± 2 Ma, 274 ± 1 Ma and 271 ± 1 Ma~ 282 ± 1 Ma, respectively. The quartz diorite shows typical features of HMA and may be formed by melting of the subcontinental lithospheric mantle wedge induced by fluids released from partial melting of the subducted oceanic crust. The source of the studied granodiorite and biotite granite might be related to partial melting of juvenile crustal materials. Considering the regional geology, we infer that the Late Palaeozoic intrusions from the south of Xiwuqi were likely emplaced during the northward subduction of the Paleo-Asian Ocean plate beneath the southern Mongolian terrane. The Early Carboniferous quartz diorites are components of a continental arc-related magmatism, the Early Permian granodiorites and biotite granites are products of magmatism in a temporal back-arc extension setting during the northward subduction.

Key words: Xing-Meng orogenic belt; Late Palaeozoic; arc-related magmatism; Hf isotope; subduction; geochemistry; geochronology.

基金项目: 中国地质调查局地质调查项目(No. 1212011085490)。

作者简介: 刘敏(1991—), 男, 博士研究生, 主要从事矿物学、岩石学、矿床学专业研究。ORCID: 0000-0002-9784-9996. E-mail: liumin6364@163.com

* 通讯作者: 张达, ORCID: 0000-0001-7145-8850. E-mail: zhangda@cugb.edu.cn

引用格式: 刘敏, 赵洪涛, 张达, 等, 2017. 内蒙古西乌旗南部晚古生代侵入岩年代学、地球化学特征及地质意义. 地球科学, 42(4): 527—548.

古生代以来,古亚洲洋的俯冲—消减过程造就了横亘于西伯利亚板块与塔里木及华北板块之间的全球规模最大的显生宙增生型造山带之一中亚造山带(Kovalenko *et al.*, 2004; Windley *et al.*, 2007; Xiao *et al.*, 2009, 2015; Wilhem *et al.*, 2012) (The Central Asian orogenic belt) (Jahn *et al.*, 2004a). 带内广泛分布的古生代蛇绿岩、俯冲—增生杂岩、岛弧、微陆块及复杂的岩浆作用与整个古亚洲洋的演化历程密切相关,长期以来倍受国内外学者关注(Sengör *et al.*, 1993; 邵济安等, 1997; 李锦轶, 1998; Xiao *et al.*, 2003; Jian *et al.*, 2008; Xu *et al.*, 2013a; Kröner *et al.*, 2014; Wilde, 2015; 王树庆等, 2016). 兴蒙造山带属于中亚造山带南东段,以大规模具正 $\epsilon_{\text{Nd}}(t)$ 和 $\epsilon_{\text{Hf}}(t)$ 值(Han *et al.*, 1997; Jahn *et al.*, 2004b; Chen *et al.*, 2009)的年轻地壳增厚为特征,记录了区内古生代以来若干微陆块之间、微陆块与南北两侧块体的多阶段拼接历程(Wu *et al.*, 2007; Zhou *et al.*, 2011, 2013). 关于古亚洲洋最终闭合的位置、时代及过程是兴蒙造山带研究中尚未解决的重要课题之一. 尽管越来越多的学者倾向于支持古亚洲洋沿索伦—西拉木伦结合带最终闭合的观点(Tang, 2002; Xiao *et al.*,

2003; Li, 2006; 陈斌等, 2009; Jian *et al.*, 2010; Eizenhöfer *et al.*, 2015),但关于最终闭合时代仍存在不同的认识,如晚泥盆世—早石炭世(Hong *et al.*, 1995; Tang, 2002; Shi *et al.*, 2004; 周志广等, 2010; Xu *et al.*, 2013a; Zhang *et al.*, 2014b)、二叠纪—三叠纪(Chen *et al.*, 2000; Xiao *et al.*, 2003; Li, 2006; Zhang *et al.*, 2007, 2008a; Miao *et al.*, 2008; 李益龙等, 2012; Liu *et al.*, 2013)等. Xu *et al.*(2013a)提出古亚洲洋被松辽—浑善达克微陆块分隔为南、北两部分,南、北洋分支分别闭合于晚志留世和晚泥盆世并形成了南造山带和北造山带,而 Jian *et al.*(2008, 2010)则认为南、北造山带应形成于弧—陆碰撞作用,古亚洲洋板块于晚石炭世再次向华北板块之下俯冲,最闭合于晚二叠世. 此外,近年来的一些研究成果表明古亚洲洋闭合过程为沿索伦—西拉木伦带向南北两侧双向俯冲(Xiao *et al.*, 2003, 2009; Eizenhöfer *et al.*, 2014; Li *et al.*, 2014; Zhang *et al.*, 2014a).

晚古生代是古亚洲洋俯冲消减的关键时期,兴蒙造山带内广泛发育的晚古生代岩浆岩(图 1a)的岩石组合类型及时空分布特征可作为揭示古亚洲洋俯冲消减过程及兴蒙造山带构造演化提供了有力线

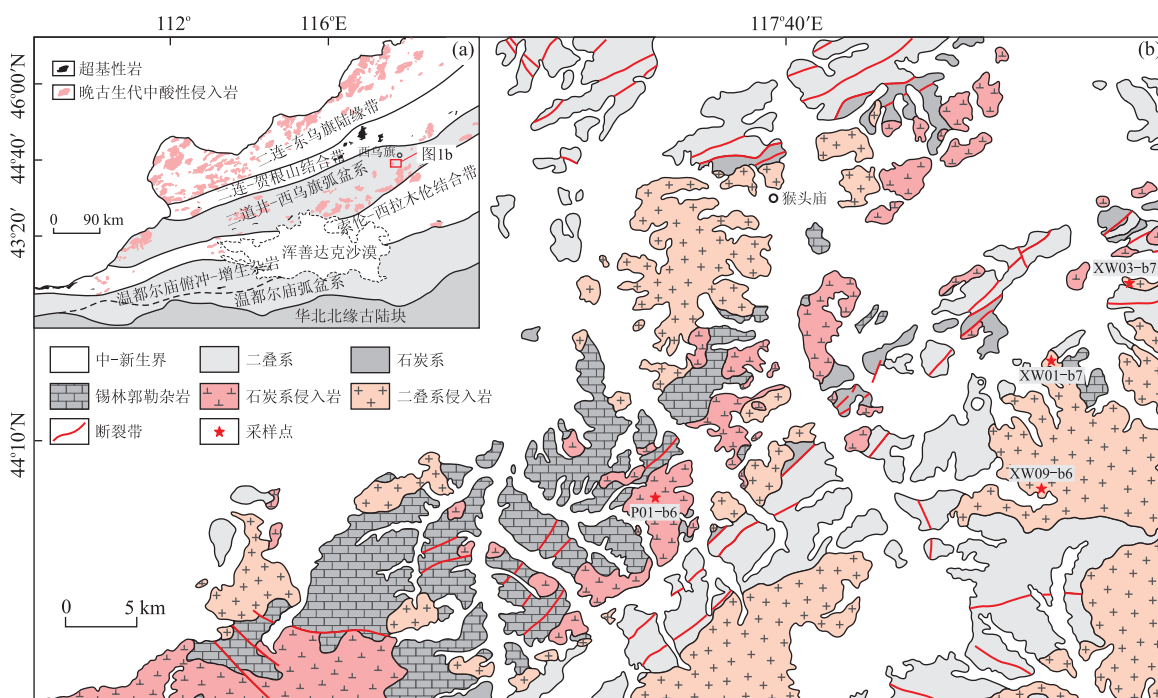


图 1 研究区地质简图

Fig. 1 Geological sketch of research area

a. 内蒙古中部构造格局示意图,据 Jian *et al.* (2008) 及索伦山—锡林郭勒 1:50 万区域地质图改编;b. 西乌旗南部达青牧场地区地质简图,据内蒙古西乌珠穆沁旗幅 1:20 万地质图改编

索。虽然兴蒙造山带内晚古生代岩浆岩的各类研究成果日趋丰富(Xiao *et al.*, 2003; Shi *et al.*, 2004; Jian *et al.*, 2008; 张晓晖和翟明国, 2010; Xu *et al.*, 2013a; 石玉若等, 2014; Chen *et al.*, 2015; Tong *et al.*, 2015),但关于岩浆成因及构造背景至今仍争议颇多。就兴蒙造山带中部而言,Zhang *et al.*(2007, 2009)认为华北板块北缘存在一条晚古生代安第斯型陆缘弧,且古亚洲洋的最终闭合应发生于二叠纪之后;Zhang *et al.*(2008b, 2011)认为锡林浩特地区早二叠世双峰式岩浆活动应代表该时期区域上已处于后碰撞伸展阶段;而Jian *et al.*(2008, 2010)则根据索伦构造带内蛇绿岩的年代学及岩石地球化学特征,利用一个完整的洋内沟—弧体系来解释二叠纪以来区域的构造—岩浆事件,并认为陆陆碰撞应发生在中二叠世(271~260 Ma)。

本文结合区域上已有的研究成果,通过对西乌旗南部晚古生代中酸性侵入岩开展LA-ICP-MS锆石U-Pb年代学、岩石地球化学及Hf同位素分析,探讨该地区晚古生代岩浆活动的时代、成因及构造背景,进一步为古亚洲洋演化及兴蒙造山带的构造格局的研究提供新信息。

1 地质背景与样品特征

研究区位于内蒙古西乌旗南部达青牧场一带,夹持于二连—贺根山蛇绿岩带与索伦—西拉木伦蛇绿岩带之间(图1a)。锡林郭勒杂岩为研究区内最老的地质体,主要为以宝音图群($Pt_{2, xl}$)、布龙山组(Obl)为主的变质岩系,出露于达青牧场北西侧(图1b)。岩相学及年代学研究表明,宝音图群为一套岛弧—陆缘弧变质沉积岩系,锡林浩特微陆块为其主要的物源区(周文孝和葛梦春, 2013; 李宝霞, 2014),而布龙山组则为一套形成于洋壳俯冲—消减阶段的变质弧前沉积建造(薛怀民等, 2009; Li *et al.*,

al., 2011; 李宝霞, 2014)。研究区内石炭系碎屑岩、碳酸盐岩及二叠系火山—沉积岩系均不整合出露于锡林郭勒杂岩之上,区内缺失三叠系(图1b)。上述所有地层单元均被侏罗系—白垩系陆相沉积及第四系不整合覆盖。

研究区内晚古生代岩浆活动十分发育,以中酸性岩为主,其分布受区域构造的控制而呈北东向,时代主要集中于晚石炭世至二叠纪(图1b)。其中区内晚石炭世岩体被部分学者(刘建峰等, 2009; Chen *et al.*, 2009)认为是苏左旗宝力道岩浆弧的东延部分。二叠纪岩体主要为二长花岗岩、正长花岗岩、花岗闪长岩及花岗岩等,Zhang *et al.*(2008b)认为该时代岩体主要形成于后碰撞伸展环境,为该地区双峰式岩浆作用的组成部分。此外,研究区南部还出露少量晚侏罗世中粗粒花岗岩。

本次研究样品石英闪长岩(P01)采自达青牧场西南部,花岗闪长岩(XW01)与黑云母花岗岩(XW03,XW09)采自前进厂地区(图1b),均与锡林郭勒杂岩侵入接触。石英闪长岩整体呈灰绿色,中细粒结构,块状构造,岩石受后期应力作用发育节理,产状约 $235^{\circ}\angle 35^{\circ}$,主要矿物为石英(10%~15%)、斜长石(65%~70%)、角闪石(10%~15%)、钾长石(8%~1%),少量辉石及磁铁矿,其中斜长石绢云母化较严重(图2a)。花岗闪长岩呈灰白色,中细粒结构,块状构造,岩体局部见少量细粒暗色捕掳体,主要矿物为石英(15%~20%)、斜长石(50%~55%)、钾长石(10%~15%)、黑云母(5%~10%),少量石榴子石、金云母及磁铁矿等(图2b)。黑云母花岗岩风化面灰褐色,新鲜面灰白色,中粗粒花岗结构,块状构造,局部亦有类似于花岗闪长岩中的暗色捕掳体产出,主要矿物为石英(20%~25%)、斜长石(45%~50%)、钾长石(18%~23%)及黑云母(8%~12%),亦含少量石榴子石、白云母、磁铁矿等(图2c, 2d)。

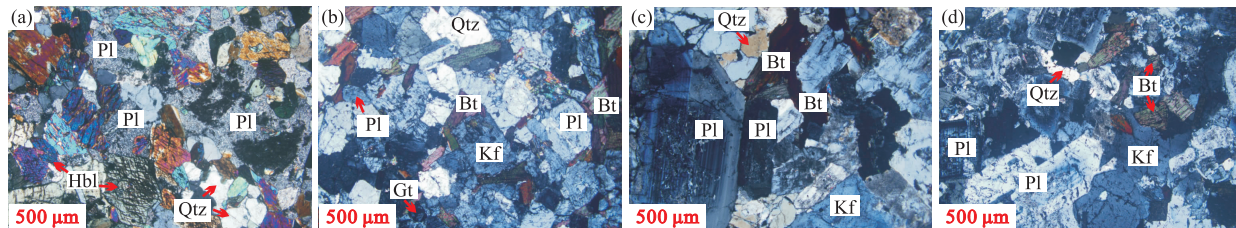


图2 研究区典型矿物样品的显微镜下(正交偏光)照片

Fig. 2 Photomicrographs (crossed nicols) of the typical mineral samples in research area
石英闪长岩(a, P01)、花岗闪长岩(b, XW01)及黑云母花岗岩(c, XW03; d, XW09)

2 实验方法

2.1 LA-ICP-MS 锆石 U-Pb 定年

本次工作分别对石英闪长岩(P01-b6)采自达青牧场西南部,花岗闪长岩(XW01-b7)与黑云母花岗岩(XW03-b7、XW09-b7)4件新鲜样品进行了年代学分析,采样点位置见图1b。锆石的分选由河北省廊坊市物化探研究所通过人工重砂分选而完成。然后在双目镜下将晶形完好、透明度较高且无裂隙或无包裹体的锆石颗粒固定在环氧树脂样靶之上,并打磨、抛光。锆石的制靶及阴极发光(CL)图像均由中科院地质与地球物理研究院完成,CL成像分析采用CAMECA SX100型电子探针,工作条件为15~20 nA电流及15 kV加速电压。

样品P01-b6的U-Pb锆石定年及微量元素分析在中国地质大学(武汉)地质过程与矿产资源国家重点实验室采用MicroLas GeoLas2005激光剥蚀系统与Agilent 7500a电感耦合等离子质谱完成,激光剥蚀束斑直径为32 μm,载气为He,工作电压为27.1 kV,激光能量密度为29 J/cm²。U-Pb定年采用标准锆石91500作外标进行同位素分馏校正,锆石微量元素含量以多个USGS参考玻璃(BCR-2G,BIR-1G)为外标、²⁹Si为内标进行定量计算。其余3件样品(XW01-b7、XW03-b7、XW09-b7)的U-Pb锆石定年由天津矿产地质调查研究所完成,分析所用仪器为Finnigan Neptune型ICP-MS及New Wave 193 nm激光器,束斑直径为35 μm,以91500及GJ-1作为外标进行U-Pb同位素分馏校正。详细的实验过程描述与数据处理方法参见Liu et al. (2008, 2010),普通Pb的校正参见Andersen(2002),加权平均年龄的计算及谐和图的绘制均采用Isoplot 3.0软件(Ludwig, 2003)完成。

2.2 Lu-Hf 同位素分析

样品P01-b6的Lu-Hf同位素原位分析测试在中国地质大学(武汉)地质过程与矿产资源国家重点实验室Neptune型多接收等离子体质谱仪上进行,激光剥蚀系统为GeoLas2005。具体分析方法和仪器参数详见Wu et al. (2006)。利用¹⁷⁶Lu/¹⁷⁵Lu=0.02655(Biévre and Taylor, 1993)和¹⁷⁶Yb/¹⁷²Yb=0.58560(Chu et al., 2002)进行同质异位干扰校正并计算样品¹⁷⁶Lu/¹⁷⁷Hf和¹⁷⁶Hf/¹⁷⁷Hf比值。样品测定以标准锆石GJ-1作为外标,分析过程中GJ-1的¹⁷⁶Hf/¹⁷⁷Hf测试加权平均值为0.282010±0.000007(2σ, n=36)。具体分析方法

和参数参见Yuan et al. (2008)。数据处理中,ε_{Hf}(t)计算采用的¹⁷⁶Lu衰变常数以及球粒陨石¹⁷⁶Hf/¹⁷⁷Hf和¹⁷⁶Lu/¹⁷⁷Hf比值参见Söderlund et al. (2004)和Blichert-Toft and Albarède(1997),亏损地幔模式年龄(T_{DM})及二阶段模式年龄(T_{DM2})计算采用的¹⁷⁶Hf/¹⁷⁷Hf和¹⁷⁶Lu/¹⁷⁷Hf比值参见Griffin et al. (2000, 2002)。

2.3 岩石地球化学分析

16件样品的主、微量元素含量分析测试在核工业北京地质研究院分析测试中心完成。主量元素分析采用XRF法(3080E),所用仪器为Philips PW2404X射线荧光光谱仪,X射线管电压为50 kV,电流为50 mA,元素测定精度可达0.01%,分析误差小于5%;FeO和烧失量分析采用标准湿化学分析法,测定范围大于0.5%。微量元素分析采用Finnigan MAT Element I型电感耦合等离子体质谱仪完成,工作温度为20 °C,相对湿度为30%。微量元素含量利用USGS标准W-2和G-2及国标GSR-1、GSR-2及GSR-3进行校正,相对误差小于10%。

3 实验结果

3.1 锆石 U-Pb 年龄

U-Pb测试数据结果见表1。4件测年样品中挑选出来的锆石大部分呈长柱状,长宽比变化较大,粒径约80~200 μm,CL图像中均显示较清晰的韵律环带结构(图3),Th/U值变化范围为0.13~2.66,应属岩浆成因锆石(Hoskin and Black, 2000)。石英闪长岩P01-b6(44°07'53.9"N, 117°33'13.8"E)19个分析点均落于谐和线上或其附近(图4),加权平均年龄值为330.1±1.9 Ma(MSWD=0.03)。花岗闪长岩XW01-b7(44°13'14.7"N, 117°54'09.8"E)共进行了21个测点分析,除8、11和14号外(可能为捕获锆石锆石),其余18个分析点的²⁰⁶Pb/²³⁸U表面年龄集中在273~275 Ma,但其中9个测点并未落到谐和线上(图4),故计算年龄值时未统计在内,其余9个测点的加权平均年龄值为273.8±1.1 Ma(MSWD=0.27)。黑云母花岗岩XW03-b7(44°16'04.8"N, 117°58'03.7"E)进行了20个测点分析,其中18个测点的²⁰⁶Pb/²³⁸U表面年龄为280~283 Ma,其余两个测点(13、14号)年龄值相对较老,而10个较好的落于谐和线上的测点给出的加权平均年龄值为281.8±1.2 Ma(MSWD=0.16)。

表1 内蒙古西乌旗地区南部侵入岩锆石U-Pb数据

Table 1 U-Pb isotopic compositions of intrusions from the south of Xiuwuqi, Inner Mongolia

样号及 测点	含量(10^{-6})		同位素比值				年龄(Ma)					
	Pb	U	$^{206}\text{Pb}/^{238}\text{U}$	$^{207}\text{Pb}/^{235}\text{U}$	$^{207}\text{Pb}/^{206}\text{Pb}$	1σ	$^{206}\text{Pb}/^{238}\text{U}$	1σ	$^{207}\text{Pb}/^{235}\text{U}$	1σ	$^{207}\text{Pb}/^{206}\text{Pb}$	1σ
P01-b6-1	791	1780	0.052 2	0.001 1	0.394 4	0.018 4	0.054 8	0.002 4	328	7	338	13
P01-b6-2	120	657	0.052 9	0.001 3	0.411 1	0.025 4	0.059 4	0.003 9	332	8	350	18
P01-b6-3	765	1989	0.052 3	0.001 1	0.393 7	0.018 0	0.054 1	0.002 3	329	7	337	13
P01-b6-4	305	1366	0.052 5	0.001 3	0.410 0	0.021 8	0.056 8	0.002 8	330	8	349	16
P01-b6-5	149	686	0.052 4	0.001 3	0.431 2	0.029 9	0.060 5	0.004 1	330	8	364	21
P01-b6-6	120	628	0.052 8	0.001 0	0.426 7	0.024 8	0.059 9	0.003 6	331	6	361	18
P01-b6-7	685	1369	0.052 2	0.000 9	0.387 3	0.022 2	0.054 5	0.003 1	328	6	332	16
P01-b6-8	199	779	0.052 5	0.001 0	0.403 4	0.023 5	0.055 7	0.003 1	330	6	344	17
P01-b6-9	352	1150	0.052 5	0.000 8	0.405 7	0.019 3	0.056 8	0.002 8	330	5	346	14
P01-b6-10	105	574	0.053 5	0.001 0	0.440 8	0.024 8	0.060 5	0.003 3	336	6	371	17
P01-b6-11	353	932	0.053 3	0.001 1	0.399 8	0.022 5	0.056 8	0.003 5	335	7	342	16
P01-b6-12	369	1596	0.053 4	0.000 8	0.399 3	0.020 3	0.055 5	0.003 1	335	5	341	15
P01-b6-13	301	1058	0.052 1	0.000 8	0.364 6	0.019 9	0.051 0	0.002 8	327	5	316	15
P01-b6-14	66	318	0.054 1	0.001 2	0.477 1	0.037 1	0.067 0	0.005 3	340	7	396	26
P01-b6-15	172	634	0.052 3	0.000 9	0.428 3	0.023 5	0.059 4	0.003 4	329	6	362	17
P01-b6-16	132	504	0.051 9	0.001 3	0.439 0	0.031 3	0.062 4	0.004 4	326	8	370	22
P01-b6-17	101	539	0.052 4	0.001 0	0.379 4	0.022 6	0.052 5	0.003 1	329	6	327	17
P01-b6-18	470	1457	0.051 7	0.000 8	0.356 3	0.015 6	0.049 7	0.002 2	325	5	309	12
P01-b6-19	536	1162	0.052 0	0.001 2	0.394 4	0.031 7	0.055 2	0.004 5	327	7	338	23
XW01-b7-1	23	441	0.043 2	0.000 3	0.497 6	0.015 8	0.083 5	0.002 5	273	2	410	13
XW01-b7-2	22	444	0.043 3	0.000 3	0.470 1	0.015 3	0.078 7	0.002 5	273	2	391	13
XW01-b7-3	16	349	0.043 3	0.000 3	0.430 4	0.025 6	0.072 1	0.004 1	273	2	363	22
XW01-b7-4	26	557	0.043 3	0.000 3	0.571 2	0.018 6	0.095 8	0.002 9	273	2	459	15
XW01-b7-5	18	396	0.043 4	0.000 3	0.309 4	0.011 7	0.051 7	0.001 9	274	2	274	10
XW01-b7-6	32	676	0.043 3	0.000 2	0.434 9	0.013 9	0.072 9	0.002 3	273	2	367	12
XW01-b7-7	30	605	0.043 2	0.000 3	0.441 6	0.014 5	0.074 2	0.002 4	273	2	371	12
XW01-b7-8	21	327	0.050 9	0.000 3	0.705 6	0.017 7	0.100 5	0.002 5	320	2	542	14
XW01-b7-9	31	625	0.043 3	0.000 3	0.547 0	0.019 4	0.091 6	0.003 1	273	2	443	16
XW01-b7-10	18	398	0.043 2	0.000 2	0.308 6	0.011 0	0.051 8	0.001 8	273	2	273	10
XW01-b7-11	20	323	0.053 5	0.000 4	0.653 2	0.021 4	0.088 5	0.002 8	336	2	510	17
XW01-b7-12	14	364	0.043 6	0.000 3	0.418 7	0.038 8	0.070 3	0.006 5	273	2	355	33
XW01-b7-13	17	365	0.043 4	0.000 3	0.308 7	0.012 8	0.051 6	0.001 2	274	2	273	11
XW01-b7-14	24	456	0.047 6	0.000 3	0.485 7	0.015 7	0.073 9	0.002 4	300	2	402	13
XW01-b7-15	22	456	0.043 2	0.000 3	0.406 4	0.015 3	0.068 2	0.002 6	273	2	346	13
XW01-b7-16	17	364	0.043 6	0.000 3	0.309 6	0.017 9	0.051 5	0.002 9	275	2	274	16
XW01-b7-17	32	739	0.043 3	0.000 3	0.308 8	0.007 2	0.051 7	0.001 2	273	2	273	6
XW01-b7-18	18	404	0.043 4	0.000 3	0.308 9	0.016 0	0.051 6	0.002 7	274	2	273	14
XW01-b7-19	23	502	0.043 6	0.000 3	0.308 8	0.018 9	0.051 3	0.003 1	275	2	273	17
XW01-b7-20	18	415	0.043 2	0.000 3	0.308 5	0.017 0	0.051 8	0.002 8	273	2	273	15
XW01-b7-21	28	623	0.043 4	0.000 3	0.308 9	0.009 9	0.051 6	0.001 6	274	2	273	9
XW03-b7-1	15	305	0.044 5	0.000 3	0.318 6	0.019 4	0.051 9	0.003 1	281	2	281	17
XW03-b7-2	11	215	0.044 5	0.000 3	0.514 5	0.021 3	0.083 8	0.003 4	281	2	421	17

续表 1

样号及 测点	含量(10^{-6})		同位素比值						年龄(Ma)					
	Pb	U	$^{206}\text{Pb}/^{238}\text{U}$	1σ	$^{207}\text{Pb}/^{235}\text{U}$	1σ	$^{207}\text{Pb}/^{206}\text{Pb}$	1σ	$^{206}\text{Pb}/^{238}\text{U}$	1σ	$^{207}\text{Pb}/^{235}\text{U}$	1σ	$^{207}\text{Pb}/^{206}\text{Pb}$	1σ
XW03-b7-3	19	397	0.0445	0.0003	0.4597	0.0168	0.0749	0.0027	281	2	384	14	1066	72
XW03-b7-4	18	411	0.0446	0.0003	0.3228	0.0213	0.0524	0.0034	282	2	284	19	305	149
XW03-b7-5	10	227	0.0445	0.0003	0.3208	0.0151	0.0523	0.0024	281	2	283	13	298	106
XW03-b7-6	14	310	0.0446	0.0003	0.3217	0.0146	0.0523	0.0024	281	2	283	13	299	103
XW03-b7-7	13	290	0.0446	0.0003	0.3196	0.0131	0.0520	0.0021	281	2	282	12	284	93
XW03-b7-8	20	427	0.0447	0.0003	0.3245	0.0101	0.0527	0.0016	282	2	285	9	316	70
XW03-b7-9	14	304	0.0448	0.0004	0.3195	0.0101	0.0517	0.0017	283	2	282	9	273	75
XW03-b7-10	22	467	0.0446	0.0003	0.5002	0.0218	0.0813	0.0034	281	2	412	18	1229	83
XW03-b7-11	15	329	0.0447	0.0003	0.3202	0.0121	0.0519	0.0019	282	2	282	11	282	85
XW03-b7-12	17	362	0.0445	0.0003	0.5048	0.0210	0.0822	0.0033	281	2	415	17	1251	78
XW03-b7-13	17	339	0.0479	0.0003	0.4923	0.0165	0.0745	0.0044	302	2	406	14	1054	65
XW03-b7-14	12	252	0.0470	0.0003	0.5098	0.0287	0.0786	0.0043	296	2	418	24	1162	108
XW03-b7-15	23	542	0.0449	0.0003	0.3216	0.0091	0.0520	0.0014	283	2	285	8	285	62
XW03-b7-16	23	475	0.0446	0.0003	0.4790	0.0184	0.0780	0.0029	281	2	397	15	1146	75
XW03-b7-17	27	551	0.0445	0.0003	0.5405	0.0135	0.0881	0.0021	281	2	439	11	1385	47
XW03-b7-18	22	495	0.0448	0.0003	0.3206	0.0109	0.0519	0.0017	283	2	282	10	279	75
XW03-b7-19	22	464	0.0446	0.0003	0.4071	0.0200	0.0663	0.0033	281	2	347	17	814	104
XW03-b7-20	67	787	0.0444	0.0003	0.5459	0.0193	0.0898	0.0030	280	2	445	16	1420	65
XW09-b6-1	36	816	0.0429	0.0004	0.3065	0.0092	0.0518	0.0016	271	2	271	8	276	71
XW09-b6-2	30	684	0.0428	0.0004	0.4614	0.0186	0.0782	0.0033	270	2	385	15	1152	84
XW09-b6-3	34	790	0.0429	0.0003	0.3045	0.0084	0.0514	0.0014	271	2	270	7	260	62
XW09-b6-4	28	674	0.0429	0.0003	0.3060	0.0074	0.0518	0.0012	270	2	271	7	276	55
XW09-b6-5	45	1026	0.0428	0.0003	0.3991	0.0091	0.0676	0.0016	270	2	341	8	857	49
XW09-b6-6	34	788	0.0428	0.0003	0.3922	0.0089	0.0665	0.0015	270	2	336	8	822	47
XW09-b6-7	42	924	0.0428	0.0003	0.4819	0.0206	0.0817	0.0033	270	2	399	17	1237	80
XW09-b6-8	62	1447	0.0424	0.0003	0.3612	0.0124	0.0617	0.0020	268	2	313	11	664	69
XW09-b6-9	53	1169	0.0429	0.0003	0.3973	0.0098	0.0671	0.0016	271	2	340	8	842	49
XW09-b6-10	56	1240	0.0429	0.0003	0.3643	0.0080	0.0616	0.0013	271	2	315	7	660	45
XW09-b6-11	52	1212	0.0428	0.0003	0.3567	0.0078	0.0604	0.0013	270	2	310	7	618	45
XW09-b6-12	33	798	0.0431	0.0003	0.3071	0.0174	0.0517	0.0029	272	2	272	15	273	129
XW09-b6-13	36	807	0.0428	0.0003	0.3051	0.0130	0.0517	0.0022	270	2	270	12	272	97
XW09-b6-14	36	804	0.0428	0.0003	0.4509	0.0139	0.0764	0.0023	270	2	378	12	1105	60
XW09-b6-15	57	1230	0.0432	0.0003	0.3057	0.0062	0.0513	0.0010	273	2	271	6	256	46
XW09-b6-16	47	899	0.0487	0.0003	0.4913	0.0100	0.0731	0.0015	307	2	406	8	1017	41
XW09-b6-17	63	1390	0.0431	0.0003	0.3047	0.0077	0.0512	0.0013	272	2	270	7	252	56
XW09-b6-18	45	1003	0.0429	0.0003	0.3065	0.0115	0.0518	0.0019	271	2	271	10	275	84
XW09-b6-19	34	699	0.0460	0.0003	0.4851	0.0153	0.0765	0.0023	290	2	402	13	1109	61
XW09-b6-20	44	1067	0.0429	0.0003	0.3060	0.0058	0.0517	0.0009	271	2	271	5	273	42

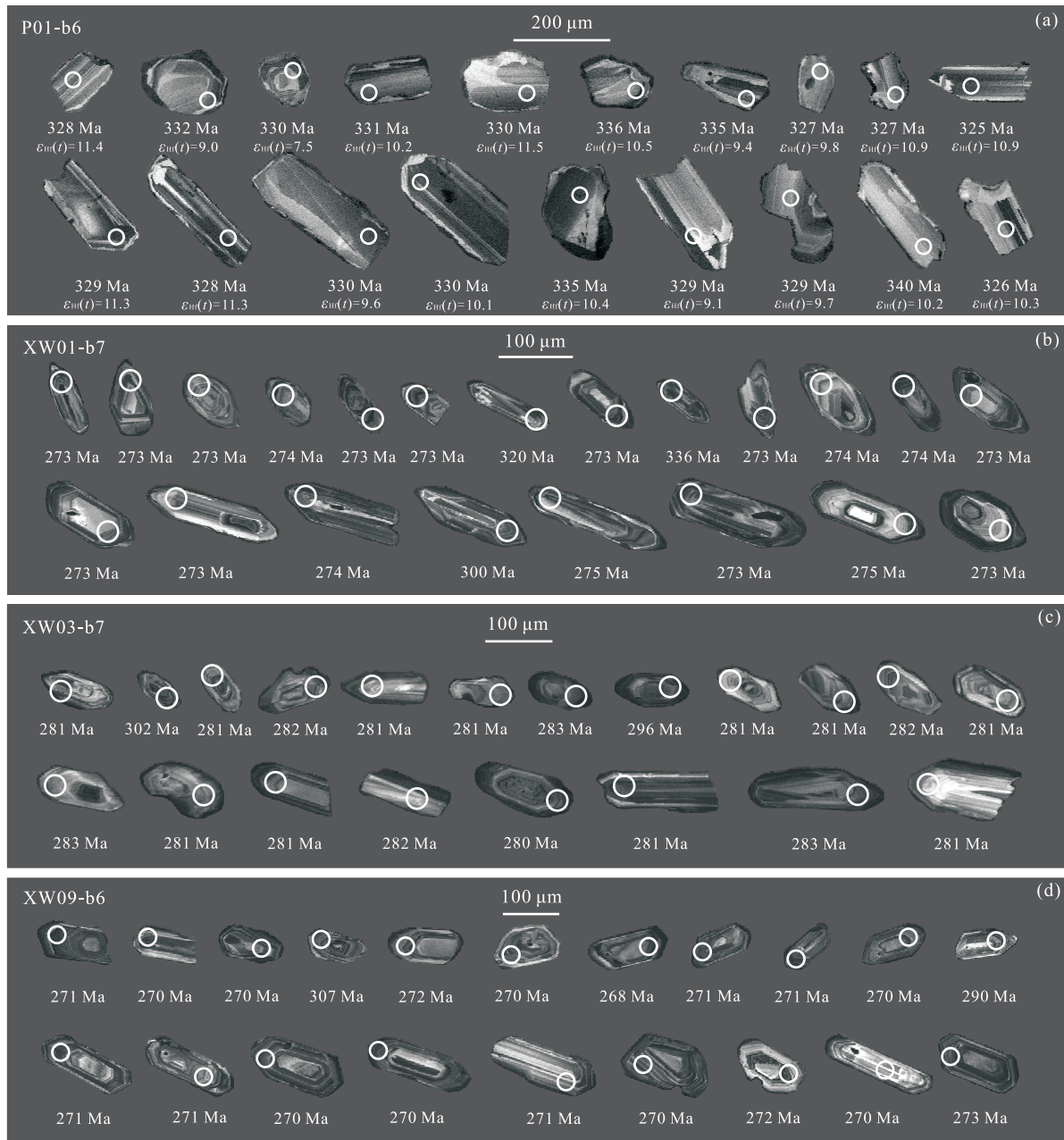


图3 石英闪长岩(a)、花岗闪长岩(b)及黑云母花岗岩(c, d)锆石阴极发光图像

Fig. 3 CL images of zircons of quartz diorite (a), granodiorite (b) and biotite granite (c, d)

(图4). 黑云母花岗岩 XW09-b6 ($44^{\circ}07'50.2''N$, $117^{\circ}53'20.2''E$)的20个分析点中,除16和19号之外,其余18个的 $^{206}\text{Pb}/^{238}\text{U}$ 表面年龄均介于在268~272 Ma,9个谐和线上的测点的加权平均年龄值为 271.3 ± 1.3 Ma(MSWD=0.17)(图4). 上述U-Pb锆石测年结果表明,研究区石英闪长岩应形成于早石炭世晚期,而花岗闪长岩及黑云母花岗岩为早二叠世晚期岩浆活动的产物.

3.2 Hf同位素分析结果

石英闪长岩 P01-b6 的锆石原位 Hf 同位素分析

结果见表2.19个分析点 $^{176}\text{Lu}/^{177}\text{Hf}$ 值为0.000 400~0.002 796,表明岩体的锆石仅存在极少量放射性成因Hf积累(Zheng *et al.*, 2007).同时 $f_{\text{Lu/Hf}}$ 值(-0.99~-0.92)也明显低于镁铁质地壳和硅铝质地壳,因此其两阶段模式年龄(T_{DM2})能够指示源区物质从地幔中分离出来的时限(Vervoort *et al.*, 1996; Amelin *et al.*, 1999).石英闪长岩锆石的初始 $^{176}\text{Hf}/^{177}\text{Hf}$ 值为0.282 782~0.282 908, $\epsilon_{\text{Hf}}(t)$ 值为7.47~11.53(图5),亏损地幔模式年龄(T_{DM})及二阶段模式年龄(T_{DM2})分别为500~659 Ma,568~794 Ma.

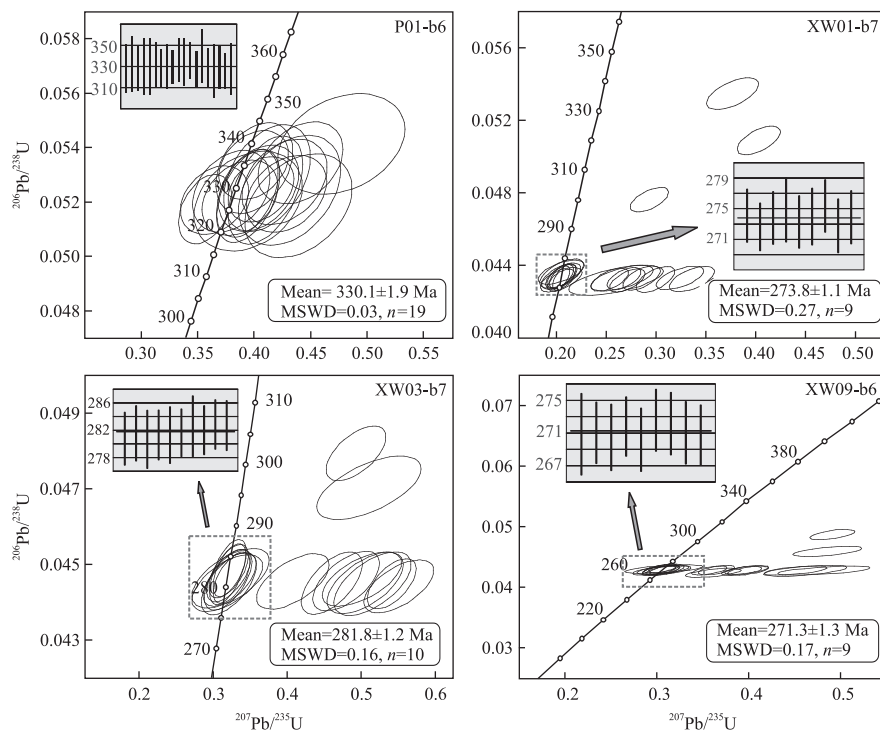


图 4 研究区石英闪长岩(P01-b6)、花岗闪长岩(XW01-b7)及黑云母花岗岩(XW03-b7、XW09-b6)锆石 U-Pb 年龄谐和图和加权年龄平均值

Fig. 4 Zircon U-Pb concordia diagrams and histograms for the investigated intrusions, P01-b6, quartz diorite; XW01-b7, granodiorite; XW03-b7 and XW09-b6, biotite granite

表 2 内蒙古西乌旗南部石英闪长岩锆石 Hf 同位素分析结果

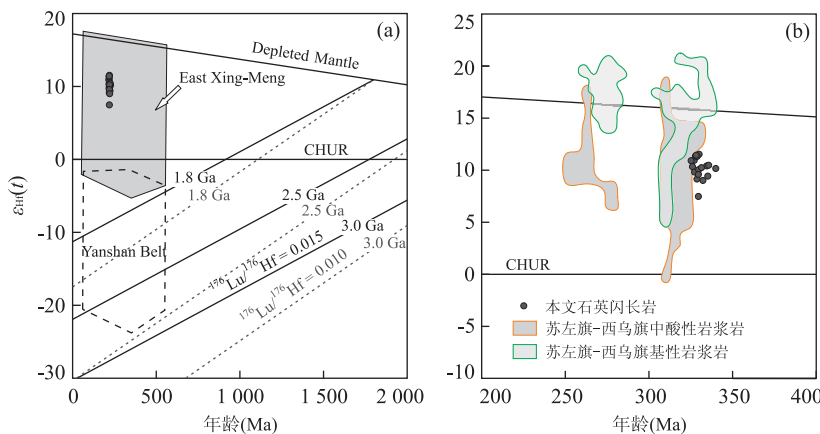
Table 2 Zircon Hf isotopic compositions of the studied quartz diorite from the south of Xiwuqi, Inner Mongolia

测点	$^{176}\text{Hf}/^{177}\text{Hf}$	1σ	$^{176}\text{Lu}/^{177}\text{Hf}$	1σ	$^{176}\text{Yb}/^{177}\text{Hf}$	1σ	$\epsilon_{\text{Hf}}(0)$	$\epsilon_{\text{Hf}}(t)$	T_{DM1} (Ma)	T_{DM2} (Ma)	$f_{\text{Lu/Hf}}$
P01-b6-1	0.282 908	0.000 025	0.002 796	0.000 071	0.082 085	0.001 746	4.8	11.4	512	572	-0.92
P01-b6-2	0.282 823	0.000 012	0.000 438	0.000 003	0.011 239	0.000 129	1.8	9.0	599	711	-0.99
P01-b6-3	0.282 898	0.000 013	0.001 685	0.000 049	0.051 237	0.001 734	4.5	11.3	511	579	-0.95
P01-b6-4	0.282 782	0.000 011	0.000 622	0.000 001	0.017 449	0.000 109	0.4	7.5	659	794	-0.98
P01-b6-5	0.282 841	0.000 014	0.000 486	0.000 005	0.012 973	0.000 123	2.4	9.6	575	676	-0.99
P01-b6-6	0.282 861	0.000 009	0.000 826	0.000 021	0.023 063	0.000 680	3.1	10.2	552	641	-0.98
P01-b6-7	0.282 897	0.000 017	0.001 315	0.000 042	0.039 303	0.001 404	4.4	11.3	508	576	-0.96
P01-b6-8	0.282 897	0.000 011	0.000 745	0.000 009	0.020 023	0.000 194	4.4	11.5	500	568	-0.98
P01-b6-9	0.282 859	0.000 014	0.001 277	0.000 018	0.036 432	0.000 643	3.1	10.1	561	650	-0.96
P01-b6-10	0.282 862	0.000 011	0.000 493	0.000 004	0.012 579	0.000 075	3.2	10.5	545	632	-0.99
P01-b6-11	0.282 862	0.000 013	0.000 577	0.000 021	0.015 518	0.000 659	3.2	10.4	547	634	-0.98
P01-b6-12	0.282 834	0.000 011	0.000 638	0.000 010	0.017 048	0.000 277	2.2	9.4	587	690	-0.98
P01-b6-13	0.282 852	0.000 010	0.001 001	0.000 018	0.026 683	0.000 416	2.8	9.8	567	661	-0.97
P01-b6-14	0.282 853	0.000 011	0.000 875	0.000 029	0.023 567	0.000 763	2.9	10.2	563	653	-0.97
P01-b6-15	0.282 830	0.000 012	0.000 665	0.000 005	0.017 643	0.000 234	2.1	9.1	593	700	-0.98
P01-b6-16	0.282 866	0.000 012	0.000 845	0.000 017	0.022 197	0.000 535	3.3	10.3	544	632	-0.97
P01-b6-17	0.282 843	0.000 009	0.000 400	0.000 000	0.009 715	0.000 031	2.5	9.7	571	672	-0.99
P01-b6-18	0.282 887	0.000 013	0.001 395	0.000 055	0.037 661	0.001 570	4.1	10.9	523	599	-0.96
P01-b6-19	0.282 886	0.000 016	0.001 314	0.000 015	0.036 360	0.000 526	4.0	10.9	523	599	-0.96

3.3 岩石地球化学分析结果

主量及微量元素分析结果分别见表 3 和表 4。由于个别样品具较高的烧失量, 故需将其余的主元

素氧化物分析数据重新换算成 100%, 以消除烧失量对含量的影响, 具体换算方法见表 3。在图 6 中,

图5 石英闪长岩 $\epsilon_{\text{Hf}}(t)$ -年龄图解Fig. 5 Plot of zircon $\epsilon_{\text{Hf}}(t)$ values vs. $^{206}\text{Pb}/^{238}\text{U}$ age for the studied quartz diorite

图a中East Xing-Meng及Yanshan Belt背景值据Chen et al. (2009)、Xiao et al. (2004)和Yang et al. (2006);图b中背景值据Chen et al. (2009)、Liu et al. (2009)、Liu et al. (2011, 2013)、Hu et al. (2015)、Li et al. (2015b)、周文孝(2012)、Shi et al. (2016)

表3 内蒙古西乌旗地区南部侵入岩主量元素(%)分析结果

Table 3 Major oxide(%) composition of intrusions from the south of Xiuwuqi, Inner Mongolia

样号	SiO_2	TiO_2	Al_2O_3	Fe_2O_3	FeO	MnO	MgO	CaO	Na_2O	K_2O	P_2O_5	LOI	Total
P01-b1	55.05	0.597	13.06	2.52	5.4	0.137	8.53	10.00	1.98	0.841	0.077	1.96	99.30
P01-b2	54.04	0.551	13.52	2.60	5.5	0.142	8.58	10.14	2.01	1.010	0.075	2.01	99.31
P01-b3	54.59	0.591	12.96	2.89	5.05	0.138	8.69	10.82	1.83	0.715	0.077	1.86	99.36
P01-b6	54.16	0.565	13.17	2.87	4.95	0.139	8.62	10.96	2.08	0.723	0.079	1.91	99.39
XW01-b1	65.97	0.802	16.16	1.31	4.15	0.049	1.36	2.22	3.37	3.620	0.237	0.86	99.52
XW01-b2	63.62	0.809	16.75	1.94	4.80	0.076	1.96	1.76	3.02	3.620	0.197	1.59	99.42
XW01-b3	63.52	0.773	16.37	1.73	4.75	0.074	1.91	1.66	2.82	3.670	0.185	2.65	99.41
XW01-b7	65.43	0.800	16.54	1.48	3.61	0.060	1.55	1.92	3.25	4.170	0.250	0.85	99.06
XW03-b1	68.74	0.530	15.78	0.72	2.75	0.040	0.92	1.67	3.69	4.150	0.210	0.65	99.20
XW03-b3	68.69	0.540	15.86	0.73	2.80	0.040	0.93	1.71	3.76	3.940	0.210	0.62	99.21
XW03-b4	68.93	0.500	15.79	0.88	2.44	0.040	0.87	1.74	3.70	4.140	0.210	0.57	99.24
XW03-b5	68.18	0.550	15.49	0.89	2.68	0.040	0.92	1.73	3.62	4.130	0.210	0.67	98.44
XW09-b1	68.06	0.520	15.27	0.64	2.71	0.050	1.44	2.45	3.68	3.140	0.140	1.65	98.10
XW09-b2	69.17	0.530	15.12	0.45	2.78	0.050	1.40	1.87	3.50	3.500	0.140	1.08	98.51
XW09-b4	68.14	0.600	15.3	0.61	3.04	0.060	1.60	2.44	3.69	2.940	0.140	1.18	98.56
XW09-b6	69.59	0.520	15.28	0.64	2.68	0.050	1.40	2.02	3.56	3.330	0.130	1.05	99.20

$\text{Mg}^{\#} = 100 \times (\text{MgO}/40.304)/(\text{MgO}/40.304 + \text{Fe}_2\text{O}_3/159.691 \times 2 + \text{FeO}/71.846)$; 标准化公式: oxide = (100-total) × oxide/total + oxide (Le Maitre, 2002)(单位: %).

石英闪长岩样品点落于辉长闪长岩区域, 黑云母花岗闪长岩样品点落于花岗岩区域及花岗岩与花岗闪长岩交界处, 而花岗闪长岩样品点则均落入花岗闪长岩类区域。

石英闪长岩(P01) SiO_2 含量为 55.09%~56.06%, K_2O 、 Na_2O 和 TiO_2 含量分别为 0.73%~1.03%、1.86%~2.12% 和 0.56%~0.61%, 属准铝质钙性系列(图7). 石英闪长岩具相对较高的 MgO (8.69%~8.84%)、 Al_2O_3 (13.18%~13.77%)、 FeO^T (7.66%~7.99%)、 CaO (10.18%~11.15%) 含量及较高的 $\text{Mg}^{\#}$ 值 (66~67). 花岗闪长岩(XW01)的 SiO_2 含量为

64.55%~66.47%, Na_2O 含量为 2.89%~3.40%, K_2O 含量为 3.65%~4.21%, MgO 含量为 1.37%~1.99%, FeO^T 含量为 4.99%~6.65%, TiO_2 含量为 0.79%~0.82%, $\text{Mg}^{\#}$ 值为 31~36, 属过铝质高 K 碱一钙性系列(图7). 黑云母花岗岩(XW03、XW09)具相对较高的 SiO_2 (69.14%~70.22%)、 K_2O (2.98%~4.20%) 和 Na_2O (3.55%~3.79%) 含量, MgO (0.88%~1.62%)、 FeO^T (3.23%~3.64%)、 TiO_2 (0.50%~0.61%) 及 $\text{Mg}^{\#}$ 值 (32~44) 则相对较低, 属过铝质高 K 钙一碱性系列(图7).

表 4 内蒙古西乌旗地区南部侵入岩微量元素 (10^{-6}) 分析结果Table 4 Trace elements (10^{-6}) composition of intrusions from the south of Xiuqi, Inner Mongolia

	P01-b1	P01-b2	P01-b3	P01-b6	XW01-b1	XW01-b2	XW01-b3	XW01-b7	XW03-b1	XW03-b3	XW03-b4	XW03-b5	XW03-b1	XW09-b2	XW09-b4	XW09-b6
La	6.10	5.35	5.70	5.30	51.20	41.90	42.00	32.26	37.98	37.40	36.90	33.26	27.63	28.34	28.30	26.26
Ce	13.10	12.30	12.80	11.80	101.00	82.30	74.47	85.64	83.12	82.71	75.15	57.28	60.47	59.40	53.51	53.51
Pr	1.79	1.79	1.83	1.70	13.00	10.20	9.31	10.39	9.97	9.99	9.15	6.79	7.09	7.09	6.80	6.80
Nd	8.05	8.39	8.28	7.80	51.50	39.80	38.40	43.34	41.84	41.38	38.62	27.57	28.82	29.50	27.88	27.88
Sm	2.04	2.19	2.06	2.00	10.10	7.40	7.32	7.81	8.87	8.45	8.25	7.99	5.47	5.79	5.70	5.84
Eu	0.64	0.69	0.66	0.63	1.46	1.38	1.35	1.37	1.11	1.05	1.10	0.95	0.92	0.91	0.93	0.96
Gd	2.26	2.44	2.28	2.30	8.29	6.26	5.89	7.15	8.15	7.65	7.40	7.13	5.14	5.37	5.42	5.62
Tb	0.47	0.51	0.49	0.48	1.36	1.07	1.02	1.11	1.25	1.16	1.16	1.08	0.87	0.95	0.91	0.96
Dy	2.74	3.05	2.85	2.78	6.39	5.73	5.13	6.38	6.91	6.25	6.34	6.03	5.07	5.61	5.48	5.96
Ho	0.55	0.61	0.56	0.55	1.02	0.88	0.82	1.16	1.23	1.07	1.12	1.06	0.96	1.10	1.06	1.15
Er	1.68	1.85	1.69	1.66	2.70	2.72	2.16	3.28	3.37	2.90	2.98	2.96	2.87	3.17	3.07	3.37
Tm	0.27	0.31	0.28	0.28	0.41	0.37	0.34	0.48	0.49	0.43	0.43	0.43	0.43	0.50	0.48	0.53
Yb	1.78	2.01	1.85	1.85	2.54	2.59	2.13	2.89	3.02	2.54	2.77	2.65	2.72	3.22	2.94	3.32
Lu	0.27	0.31	0.27	0.28	0.35	0.35	0.31	0.46	0.49	0.40	0.43	0.41	0.44	0.52	0.48	0.54
Y	15.40	17.10	15.70	15.60	28.10	24.40	22.40	31.16	32.37	29.11	29.47	29.50	25.95	28.92	28.18	31.01
Rb	22.10	30.10	17.00	18.40	114.00	116.00	118.00	130.00	141.00	143.00	142.00	103.00	111.00	107.00	108.00	108.00
Ba	112.00	154.00	121.00	131.00	1078.00	941.00	990.00	1062.00	837.00	755.00	873.00	863.00	525.00	543.00	586.00	598.00
Hf	1.39	1.44	1.41	1.40	2.12	3.23	2.69	8.82	9.89	10.08	9.25	10.04	7.66	7.10	7.97	6.80
Ta	0.14	0.14	0.14	0.14	0.69	0.66	0.71	0.90	1.24	1.31	1.06	1.24	0.75	0.89	0.78	0.90
Pb	3.69	5.12	4.60	3.75	23.70	22.30	22.04	24.71	24.62	23.30	24.44	18.57	18.59	16.31	20.83	20.83
Th	1.14	0.86	1.42	0.89	17.80	13.50	11.98	13.77	12.64	11.95	13.41	9.33	9.76	9.25	10.51	10.51
U	0.33	0.31	0.52	0.29	1.69	2.43	2.23	1.62	1.72	1.65	1.59	1.86	1.31	1.40	1.19	2.11
Nb	1.97	2.00	2.05	1.84	13.70	13.40	14.00	19.29	16.51	17.03	16.29	17.90	12.28	12.10	13.28	12.72
Sr	232.00	251.00	245.00	230.00	233.00	251.00	263.00	206.00	156.00	158.00	162.00	156.00	136.00	135.00	144.00	131.00
Zr	30.00	32.40	30.70	32.40	85.00	125.00	103.00	273.00	251.00	260.00	245.00	259.00	179.00	178.00	193.00	170.00
Cr	544.00	530.00	546.00	535.00	27.30	51.10	49.10	31.30	14.70	16.80	12.70	15.10	30.70	29.00	30.80	30.60
Ni	113.00	112.00	114.00	116.00	13.00	21.10	19.70	15.14	9.64	9.09	9.46	9.13	14.16	13.66	13.22	14.32

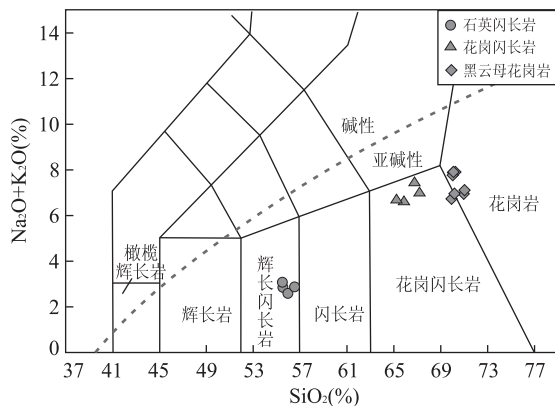


图6 研究区侵入岩 TAS 图解

Fig. 6 TAS diagram for the intrusions from our study area
据 Middlemost *et al.* (1994) 及 Irvine and Baragar(1971)

石英闪长岩(P01)样品的 Σ REE为 $39.4 \times 10^{-6} \sim 41.8 \times 10^{-6}$,在图8a中显示微右倾的配分模式,轻稀土元素相对富集,而重稀土元素略亏损(LREE/HREE=2.77~3.17).其 $(La/Yb)_N$ 、 $(La/Sm)_N$ 、 $(Gd/Yb)_N$ 分别为1.91~2.46、1.58~1.93和1.00~1.03, δEu 为0.90~0.93,表明石英闪长岩的轻重稀土分馏程度较低,同时Eu异常不明显。花岗闪长岩(XW01)的 Σ REE为 $186.5 \times 10^{-6} \sim 251.3 \times 10^{-6}$,LREE/HREE=7.14~10.26, $(La/Yb)_N$ =8.02~14.46, $(La/Sm)_N$ =2.66~3.70, $(Gd/Yb)_N$ =2.00~2.70, δEu =0.49~0.63,在图8a中表现为右倾配分模式,反映岩石相对富集轻稀土而亏损重稀土元素,其轻重稀土内部分馏不明显,具负Eu异常。两套黑云母花岗岩(XW03,XW09)样品在图8a中表现为相似的右倾配分模式,但XW03的 Σ REE为 $186.9 \times 10^{-6} \sim 212.2 \times 10^{-6}$,XW09为 $142.7 \times 10^{-6} \sim 151.8 \times 10^{-6}$.同时二者在LREE/HREE(7.52~8.12;5.65~6.79)、 $(La/Yb)_N$

(8.99~10.58;5.67~7.29)、 $(La/Sm)_N$ (2.69~2.89;2.90~3.26)、 $(Gd/Yb)_N$ (2.21~2.50;1.38~1.57)及 δEu (0.39~0.43;0.50~0.53)上的不同说明XW03黑云母花岗岩相对具更明显的轻重稀土元素分馏及Eu负异常,岩浆演化过程存在差异性。在图8b中,石英闪长岩明显富集Rb、Th、U、K等大离子亲石元素元素和活泼不相容元素,而亏损Nb、Ta等高场强元素;花岗闪长岩和黑云母花岗岩在图8b显示相似的配分模式,均强烈富集大离子亲石元素元素和活泼不相容元素(如Rb、Ba、K、Th、U等),亏损高场强元素(如Nb、Ta、Ti等),但Ba、Sr、Zr、Hf等的差异性指示出不同的岩浆演化过程。

4 讨论

4.1 成岩时代及源区性质

兴蒙造山带中部的古生代岩浆活动大都受构造线约束而呈近东西向带状展布,其中,在索伦结合带与贺根山结合带之间的二道井—西乌旗一线区域内广泛发育晚古生代中酸性侵入岩类。前人对于这些侵入岩大量的研究工作表明,石炭纪岩体以石英闪长岩、花岗闪长岩、英云闪长岩及花岗岩类为主,时代多集中在330~300 Ma(石玉若等,2014),自西向东共同构成了苏左旗—锡林浩特—西乌旗石炭纪弧岩浆岩带(Chen *et al.*, 2000; 鲍庆中等, 2007; 刘建峰等, 2009; 刘翼飞等, 2010; 周文孝, 2012; Shi *et al.*, 2016)。早二叠世花岗闪长岩、花岗岩类(周文孝, 2012; Li *et al.*, 2016a)及火山岩(Zhang *et al.*, 2008b, 2011; 刘建峰, 2009; 陈彦等, 2014; Li *et al.*, 2016a)也在西乌旗、锡林浩特等地带广泛出露。同时,区域内二叠系、三叠系沉积岩的碎屑锆石年龄均存在晚古生代的年龄峰值区间,指

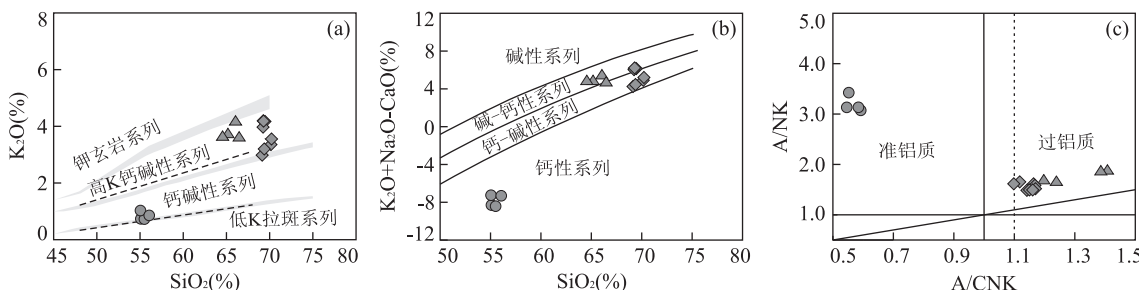
图7 研究区侵入岩 SiO₂-K₂O 图解及 A/CNK-A/NK 图解

Fig. 7 K₂O vs. SiO₂ diagram (a), modified alkali-lime index diagram (b) and A/NK vs. A/CNK diagram (c) for the studied intrusions

a. 据 Rickwood(1989); b. 据 Frost *et al.* (2001); c. 据 Peccerillo and Taylor(1976)

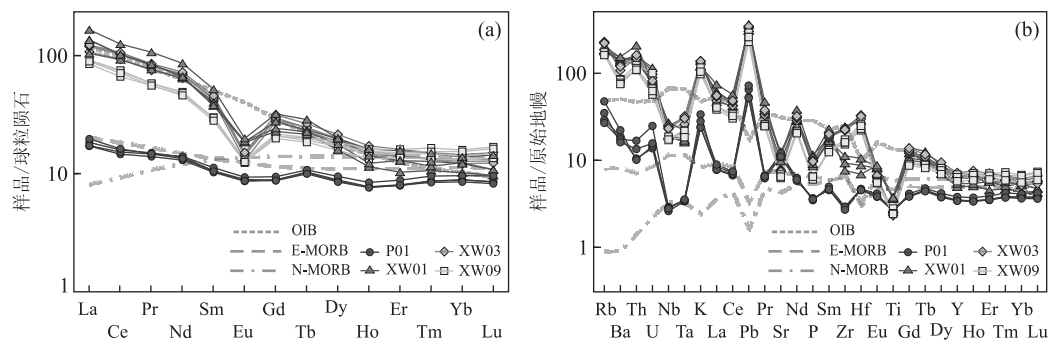


图 8 球粒陨石标准化REE图解及微量元素原始地幔标准化图解

Fig. 8 Chondrite-normalized REE patterns (a) and primitive mantle-normalized trace element patterns (b)

a. 据 Boynton(1984)及 Sun 和 McDonough(1989); b. 据 Sun 和 McDonough(1989)

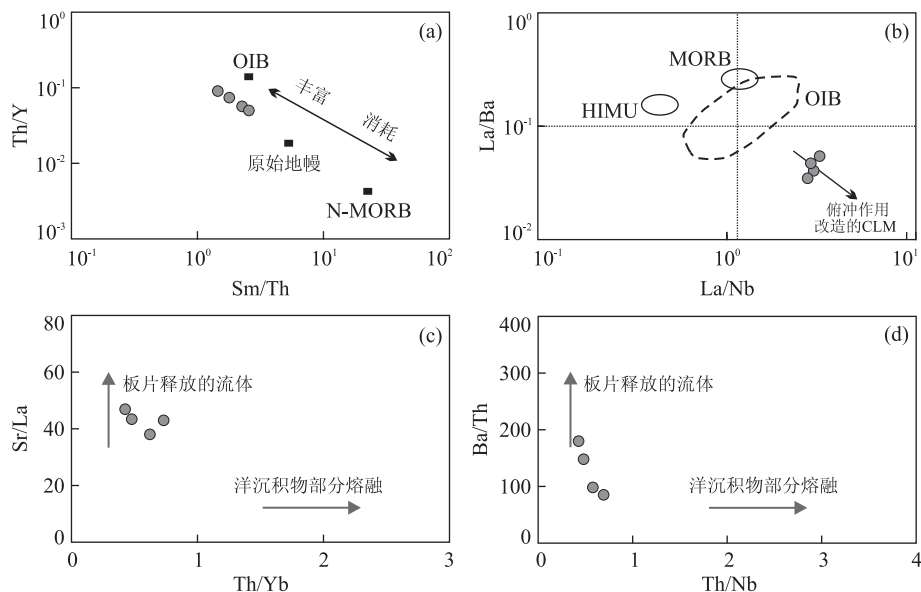


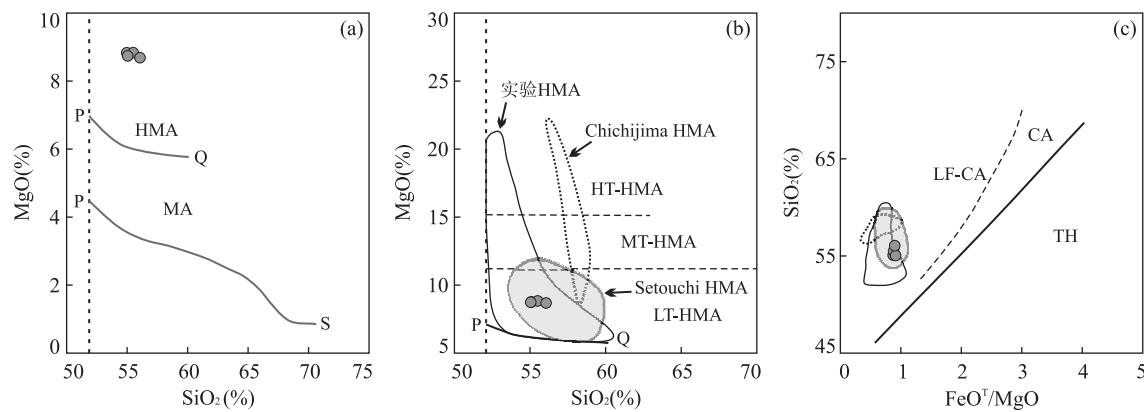
图 9 石英闪长岩 Sm/Th-Th/Y 图解(a)、La/Nb-La/Ba 图解(b)、Th/Yb-Sr/La 图解(c) 及 Th/Nb-Ba/Th 图解(d)

Fig. 9 Sm/Th-Th/Y (a), La/Nb-La/Ba (b), Th/Yb-Sr/La (c) and Th/Nb-Ba/Th (d) diagrams for the studied quartz diorite
据邓晋福等(2010); CLM, 大陆岩石圈地幔

示该时期强烈的构造—岩浆事件(Li *et al.*, 2002; Han *et al.*, 2012)。本文石英闪长岩(P01-b6)、花岗闪长岩(XW01-b7)及两件黑云母花岗岩(XW03-b7、XW09-b6)样品的锆石 U-Pb 加权平均年龄值分别为 330、274、282 及 271 Ma, 表明其分别侵位结晶于早石炭世晚期及早二叠世晚期, 与区域内的岩浆事件基本相符。

本文石英闪长岩明显富集大离子亲石元素, 亏损高场强元素(图 8b), 显示俯冲带弧岩浆岩的性质(Kelemen *et al.*, 2007), 而高的 Cr($530 \times 10^{-6} \sim 546 \times 10^{-6}$)、Ni($112 \times 10^{-6} \sim 116 \times 10^{-6}$)含量、低的 Zr($30.0 \times 10^{-6} \sim 32.4 \times 10^{-6}$)、Hf($1.39 \times 10^{-6} \sim 1.44 \times 10^{-6}$)含量及 La/Sm 值($2.44 \sim 2.99$)暗示源区无明显的地壳物质混染(Mahoney and Cof-

fin, 2013), 结合其低硅、高铁镁、高 $\epsilon_{\text{Hf}}(t)$ 值($7.47 \sim 11.53$)及年轻 T_{DM2} ($568 \sim 794$ Ma)的特点, 认为石英闪长岩主要源于幔源岩浆作用。与 N-MORB 相比, 该石英闪长岩具较高的 Th/Y 值($0.05 \sim 0.07$)和较低的 Sm/Th($1.79 \sim 2.56$)值(图 9a), 表明其地幔源区相对富集, 而相对较高的 La/Nb 值($2.68 \sim 3.10$)、La/Ta 值($38.21 \sim 42.36$)和低的 La/Ba($0.03 \sim 0.05$)值(图 9b)符合受俯冲作用改造后的大陆岩石圈地幔源区的特征(Saunders *et al.*, 1992)。俯冲带的地幔源区通常因俯冲板片的脱水作用所产生的流体或洋沉积物的参与而发生富集(Elliott, 2013), 轻稀土元素、高场强元素及 Th 可作为判定俯冲板片流体参与程度的标志(Elliott *et al.*, 1997; Pearce, 2008; Li *et al.*,

图 10 HMA SiO_2 - MgO 图解及 FeO^T/MgO - SiO_2 图解Fig. 10 SiO_2 - MgO and FeO^T/MgO - SiO_2 diagrams for HMA

PQ 及 PS 线分别为 HMA 与 MA、MA 与非 MA 分界线; HT. 高温; MT. 中温; LT. 低温; LF. 低铁; 据 Elliott *et al.* (1997)

2016b). 根据图 9c, 9d 可知, 俯冲板片脱水熔融所产生的流体是造成石英闪长岩地幔源区富集的主要因素。此外, 本文石英闪长岩具高 MgO 含量(8.69%~8.84%)、高 $\text{Mg}^{\#}$ 值(66~67)及低 FeO^T/MgO 值(0.87~0.91), 符合典型高镁闪长岩/安山岩类(HMA)的特征(邓晋福等, 2010, 2015)。由图 10 可知, 该套石英闪长岩体应属低温、低铁钙碱性系列 HMA, 类似于日本 Setouchi 新生代岛弧火山带内的 HMA(Shimoda *et al.*, 1998), 因此推测此石英闪长岩可能与俯冲洋壳板片释放的含水流体加入到上部地幔楔中而引发地幔橄榄岩熔融作用有关(Hirose, 1997; 唐功建和王强, 2010; 邓晋福等, 2010, 2015)。在西乌旗达青牧场西侧地区(刘建峰等, 2009)及锡林浩特东部(康健丽等, 2016)也存在同期的 HMA 型岩浆活动记录。

本文花岗闪长岩和黑云母花岗岩显示相似的稀土元素配分模式和微量元素特征(图 8), 且形成时代较为接近, 可能具有同源岩浆演化的特征。花岗闪长岩与黑云母花岗岩具较低的 MgO 、 CaO 、 FeO^T 、 Cr 、 Ni 含量, 同时存在明显的 Eu 负异常, 在微量元素原始地幔标准化图中明显亏损 Nb、Ta、Pb、Ti 而富集 Th、Zr、Hf 等元素, 这些特征表明其岩浆源区可能存在地壳物质的混染作用。Li *et al.* (2016a)对本研究区南侧新林镇附近的北大山花岗闪长岩(277 Ma)和沙胡同花岗闪长岩(275 Ma)的同位素分析结果显示, 该时期的岩体具较低 $\epsilon_{\text{Nd}}(t)$ 值(-0.4~3.1)、较老 Nd 模式年龄(0.91~1.21 Ga)及较高的 $\delta^{18}\text{O}$ 值(0.629‰~0.813‰), 指示明显的壳源物质混染。但北大山花岗闪长岩和沙胡同花岗闪长岩的 $\epsilon_{\text{Hf}}(t)$ 值(7.6~10.7)及 T_{DM2} (620~

820 Ma)与本文中石英闪长岩(330 Ma)极为相近, 表明研究区的早二叠世花岗闪长岩和黑云母花岗岩可能主要源于新生壳源物质的熔融作用。在 F-An-Or 三角相图(Castro, 2013)中, 花岗闪长岩及黑云母花岗岩样品点基本呈线性排布, 且靠近低压(0.3 GPa)、水不饱和(0.9% H_2O , 质量百分比)反应线(图 11), 暗示其源区可能与安山质母岩浆在低压、缺水条件下的分离结晶作用有关, 花岗闪长岩样品点的偏移可能是由少量残余体不混融或变质沉积物的同化混染作用所导致。样品明显的 Eu、Sr 负异常可能与斜长石等矿物的分离结晶有关。本文花岗闪长岩及黑云母花岗岩锆石 U-Pb 结果中均存在 300~320 Ma 的捕获锆石, 因此笔者推测其母岩浆可能来源于晚石炭世俯冲带内俯冲洋壳与上覆地幔

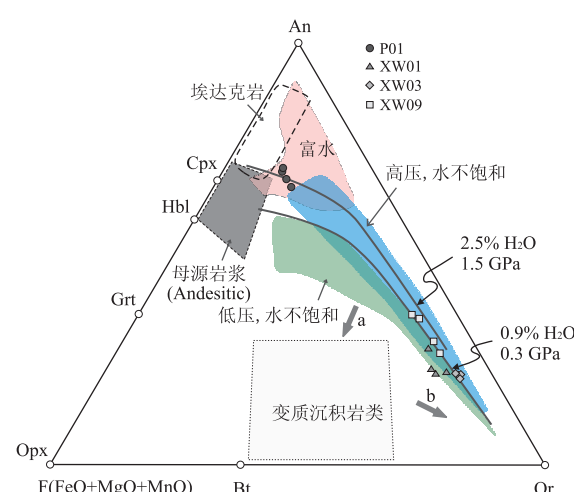


图 11 研究区侵入岩 F-An-Or 三角相图

Fig. 11 F-An-Or pseudo-ternary diagram for the studied intrusions

据 Castro(2013); a. 同化混染; b. 残余体不混融

楔形体反应后就位于下地壳的新生壳源物质的部分熔融。

4.2 构造环境分析

本文石英闪长岩为典型的 HMA 型火成岩类, 为俯冲带上面的楔形地幔在俯冲洋壳脱水条件下发生局部熔融的产物, 是苏左旗—锡林浩特—西乌旗石炭纪钙碱性弧侵入岩带(Chen *et al.*, 2000; 鲍庆中等, 2007; 刘建峰等, 2009; 刘翼飞等, 2010; 周文孝, 2012; Shi *et al.*, 2016)的组成部分。古亚洲洋在石炭纪沿索伦—西拉沐沦构造带向北侧的南蒙古微地块下持续俯冲, 在苏左旗—锡林浩特—西乌旗一线形成陆缘弧岩浆岩带, 同时沿俯冲带形成相应的俯冲—增生带, 例如达青牧场南侧晚石炭世—早二叠世俯冲—增生杂岩体(Liu *et al.*, 2013)。石英闪长岩均出露与俯冲—增生杂岩带, 进一步证实了古亚洲洋为向北俯冲。研究区石炭世中酸性岩浆活动在早期总体显示较高的 $\epsilon_{\text{Hf}}(t)$ 值(图 5b), 随着俯冲作用的持续推进, 岩浆在上升过程中可能存在古老地壳物质的混入, 致使部分岩体的 $\epsilon_{\text{Hf}}(t)$ 值发生下降, 石炭纪基性岩浆活动的 $\epsilon_{\text{Hf}}(t)$ 值也呈现类似的趋势(Chen *et al.*, 2009; 周文孝, 2012; Liu *et al.*, 2013; Shi *et al.*, 2016)。此外, 石炭系本巴图组火山岩也表现出岛弧或大陆边缘弧火山岩的特征(刘建峰, 2009; 潘世语等, 2012; 李瑞杰, 2013), 与上述钙碱性弧侵入岩带共同构成了一套活动大陆边缘火成岩组合。

关于索伦—西拉沐沦构造带北侧苏左旗至西乌旗早二叠世岩浆活动的构造环境目前仍存在较大的争议, 一种观点为古亚洲洋持续俯冲作用下的弧岩浆(Jian *et al.*, 2010; Li *et al.*, 2011; Li *et al.*, 2016a); 另一种观点为陆内裂谷或后碰撞伸展环境的板内岩浆活动(Zhang *et al.*, 2008b; 周志广等, 2010; 晨辰等, 2012; Xu *et al.*, 2013a; 王键等, 2016)。值得注意的是, 高度分离(highly fractionated)的 I 型和 S 型花岗岩在部分判别图解中也会显示 A 型花岗岩的特征(邓晋福等, 2015), 且双峰式火山岩也并不仅仅产于大陆裂谷环境(Pin and Paquette, 1997; Frost *et al.*, 1999)。索伦—西拉沐沦河北侧虽广泛出露二叠系, 但中二叠统哲斯组、上二叠统林西组中华北克拉通 1.8 Ga 左右和 2.5 Ga 左右的年龄记录极为少见(Han *et al.*, 2012; Han *et al.*, 2015; Li *et al.*, 2015a), 直至晚二叠世末期才逐渐出现华北北缘火成岩的锆石(Eizenhöfer *et al.*, 2014), 暗示早二叠世仍保留有

分隔南北板块的大洋。然而, 索伦—西拉沐沦构造带北侧具极高 $\epsilon_{\text{Hf}}(t)$ 值的早二叠世(272~275 Ma)基性岩浆活动(图 5b)(Liu *et al.*, 2011; Li *et al.*, 2015b)以及锡林浩特地区典型的早二叠世(280 Ma)双峰式火山岩(Zhang *et al.*, 2008b)均指示区域当时处于相对伸展的环境。同时, 索伦—西拉沐沦构造带北侧二叠系火山—沉积物的地球化学特征显示其形成于古亚洲洋向北俯冲时的弧后盆地环境(Eizenhöfer *et al.*, 2015)。结合上述地质事实, 笔者推测研究区在古亚洲洋俯冲晚期阶段可能经历了一次由于俯冲板片后撤(slab roll-back)而引起的弧后伸展作用过程(back-arc extension), 本文早二叠世花岗闪长岩及黑云母花岗岩或为这一阶段的产物。随着弧后扩张的进行, 软流圈地幔上涌, 导致了该时期的基性岩浆活动, 而软流圈地幔提供的热量使新增生的地壳物质再度发生熔融并侵位上升, 进而形成了本文中的早二叠世花岗闪长岩及黑云母花岗岩。短暂的弧后伸展之后, 古亚洲洋逐渐沿索伦—西拉沐沦构造带关闭, 而 270~260 Ma 左右的岩浆活动间歇期(Li *et al.*, 2002)可能标志着俯冲作用的结束。

4.3 区域构造演化

兴蒙造山带古生代的构造演化主要由古亚洲洋的演化主导, 二连—贺根山蛇绿混杂岩带、索伦—西拉沐沦蛇绿混杂岩带以及伴随的大量岩浆活动和增生带均是洋壳俯冲—消减过的产物, 并且越来越多的学者倾向于将索伦—西拉沐沦带作为古亚洲洋最终闭合的位置(Xiao *et al.*, 2003; Li, 2006; Jian *et al.*, 2008, 2010; Li *et al.*, 2016a)。

晚古生代以来, 古亚洲洋沿着索伦—西拉沐沦带向北侧的南蒙古陆块和南侧的华北板块“双向”俯冲(Xiao *et al.*, 2003, 2009; Eizenhöfer *et al.*, 2014; Li *et al.*, 2014; Zhang *et al.*, 2014a), 在华北板块北缘形成近东西向的安第斯型活动大陆边缘弧岩浆岩带(Zhang *et al.*, 2007, 2009), 同样在南蒙古陆块南缘也形成了一系列弧岩浆和俯冲增生体(Chen *et al.*, 2000; 鲍庆中等, 2007; 刘建峰等, 2009; 刘翼飞等, 2010; 周文孝, 2012; Liu *et al.*, 2013; Shi *et al.*, 2016)。Zhang *et al.*(2014a)研究人员最近沿索伦构造带完成的地震波反射剖面也揭示了双向俯冲的存在。早石炭世至早二叠世, 古亚洲洋持续向北俯冲, 在早二叠世晚期由于俯冲板片的回撤, 造成了区域内一次短暂的弧后伸展作用。最终, 古亚洲洋于晚古生代末期闭合(Chen *et al.*,

2000; Xiao *et al.*, 2003; Li, 2006; Zhang *et al.*, 2007; Miao *et al.*, 2008; Liu *et al.*, 2013),随后区域演化转为受古太平洋的俯冲作用主导(Li, 2006; Xu *et al.*, 2013b; Zhou *et al.*, 2013)。

南蒙古陆块南部绝大部分显生宙花岗岩类均具较低的 Sr 初始值和正的 $\epsilon_{\text{Nd}}(t)$ 值,指示显生宙以来显著的地壳增生。本文石炭纪至早二叠世的侵入岩及研究区同期的俯冲增生杂岩(Liu *et al.*, 2013)和其他岩浆活动(图 5b),记录了该时期古亚洲洋在向北侧南蒙古陆块俯冲时强烈的地壳增生作用。同时,弧岩浆活动由北向南逐渐变年轻的趋势、达青牧场俯冲增生杂岩向南展布以及蛇绿混杂岩带可能代表着兴蒙造山带的水平向地壳增生(Xiao *et al.*, 2003, 2009; 李锦铁等, 2009; Liu *et al.*, 2013),垂向增生主要以地幔物质和俯冲洋壳组分的参与为主(Hawkesworth *et al.*, 1997; Li *et al.*, 2016b)。

5 结论

(1) 西乌旗南部石英闪长岩、花岗闪长岩及黑云母花岗岩的结晶年龄分别 330 ± 2 Ma、 274 ± 1 Ma 及 271 ± 1 Ma~ 282 ± 1 Ma, 表明研究区在早石炭世末及早二叠世存在两期明显岩浆活动。

(2) 石英闪长岩属低温、低铁钙碱性系列 HMA,结合其较高的 $\epsilon_{\text{Hf}}(t)$ 值(7.47~11.53)和年轻的 T_{DM2} 年龄(568~794 Ma),笔者认为其形成可能与俯冲洋壳板片释放的流体加入到上覆楔形地幔后引发部分熔融有关。而花岗闪长岩及黑云母花岗岩可能形成于新生壳源物质的部分熔融后的安山质母岩浆在低压、缺水条件下的分离结晶作用有关。

(3) 研究区早石炭世末石英闪长岩形成于古亚洲洋向北侧南蒙古陆块下俯冲时的活动大陆边缘弧环境,而花岗闪长岩及黑云母花岗岩则可能侵位于俯冲过程中的短暂的弧后伸展阶段。此两期岩浆活动参与了兴蒙造山带晚古生代强烈的地壳增生过程。

致谢:野外工作得到了李瑞杰、董金元、陈诚等的大力支持,样品测试及数据分析时中国地质大学(武汉)地质过程与矿产资源国家重点实验室、天津矿产地质调查研究所工作人员给予了悉心指导,审稿专家对本文进行了细致的审阅并提出了宝贵修改意见,在此一并表示衷心的感谢!

References

- Amelin, Y., Lee, D. C., Halliday, A. N., et al., 1999. Nature of the Earth's Earliest Crust from Hafnium Isotopes in Single Detrital Zircons. *Nature*, 399 (6733): 1497–1503. doi: 10.1038/20426
- Andersen, T., 2002. Correction of Common Lead in U-Pb Analyses that do not Report ^{204}Pb . *Chemical Geology*, 192(1–2): 59–79. doi: 10.1016/S0009-2541(02)00195-X
- Bao, Q. Z., Zhang, C. J., Wu, Z. L., et al., 2007. SHRIMP U-Pb Zircon Geochronology of a Carboniferous Quartz-Diorite in Baiyingaole Area, Inner Mongolia and Its Implications. *Journal of Jilin University (Earth Science Edition)*, 37(1): 15–23 (in Chinese with English abstract).
- Biévre, P. D., Taylor, P. D. P., 1993. Table of the Isotopic Compositions of the Elements. *International Journal of Mass Spectrometry & Ion Processes*, 123(2): 149–166. doi: 10.1016/0168-1176(93)87009-H
- Blichert-Toft, J., Albarède, F., 1997. The Lu-Hf Isotope Geochemistry of Chondrites and the Evolution of the Mantle-Crust System. *Earth & Planetary Science Letters*, 148(1–2): 243–258. doi: 10.1016/S0012-821X(97)00040-X
- Boynton, W. V., 1984. Chapter 3–Cosmochemistry of the Rare Earth Elements: Meteorite Studies. *Developments in Geochemistry*, 2(2): 63–114. doi: 10.1016/B978-0-444-42148-7.50008-3
- Castro, A., 2013. Tonalite-Granodiorite Suites as Cotectic Systems: A Review of Experimental Studies with Applications to Granitoid Petrogenesis. *Earth-Science Reviews*, 124(9): 68–95. doi: 10.1016/j.earscirev.2013.05.006
- Chen, B., Jahn, B. M., Tian, W., 2009. Evolution of the Solonker Suture Zone: Constraints from Zircon U-Pb Ages, Hf Isotopic Ratios and Whole-Rock Nd-Sr Isotope Compositions of Subduction- and Collision-Related Magmas and Forearc Sediments. *Journal of Asian Earth Sciences*, 34(3): 245–257. doi: 10.1016/j.jseaes.2008.05.007
- Chen, B., Jahn, B. M., Wilde, S., et al., 2000. Two Contrasting Paleozoic Magmatic Belts in Northern Inner Mongolia, China: Petrogenesis and Tectonic Implications. *Tectonophysics*, 328(1–2): 157–182. doi: 10.1016/S0040-1951(00)00182-7
- Chen, B., Ma, X. H., Liu, A. K., et al., 2009. Zircon U-Pb Ages of the Xilinhot Metamorphic Complex and Blueschist, and Implications for Tectonic Evolution of the

- Solonker Suture. *Acta Petrologica Sinica*, 25 (12): 3123—3129 (in Chinese with English abstract).
- Chen, C., Zhang, Z. C., Guo, Z. J., et al., 2012. Geochronology, Geochemistry, and Its Geological Significance of the Permian Mandula Mafic Rocks in Damaoqi, Inner Mongolia. *Earth Science*, 42(3): 343—358 (in Chinese with English abstract).
- Chen, C., Zhang, Z. C., Li, K., et al., 2015. Geochronology, Geochemistry, and Its Geological Significance of the Damaoqi Permian Volcanic Sequences on the Northern Margin of the North China Block. *Journal of Asian Earth Sciences*, 97: 307—319. doi: 10.1016/j.jseas.2014.06.024
- Chen, Y., Zhang, Z. C., Li, K., et al., 2014. Geochronology, Geochemistry and Geological Significance of the Permian Bimodal Volcanic Rocks in Xi Ujimqin Banner, Inner Mongolia. *Acta Scientiarum Naturalium Universitatis Pekinensis*, 50(5): 843—858 (in Chinese with English abstract).
- Chu, N. C., Taloy, R. N., Chavagnac, V., et al., 2002. Hf Isotope Ratio Analysis Using Multi-Collector Inductively Coupled Plasma Mass Spectrometry: An Evaluation of Isobaric Interference Corrections. *Journal of Analytical Atomic Spectrometry*, 17(12): 1567—1574. doi: 10.1039/B206707B
- Deng, J. F., Feng, Y. F., Di, Y. J., et al., 2015. Magmatic Arc and Ocean-Continent Transition: Discussion. *Geological Review*, 61(3): 473—484 (in Chinese with English abstract).
- Deng, J. F., Liu, C., Feng, Y. F., et al., 2010. High Magnesian Andesitic/Dioritic Rocks (HMA) and Magnesian Andesitic/Dioritic Rocks (MA): Two Igneous Rock Types Related to Oceanic Subduction. *Geology in China*, 37(4): 1112—1118 (in Chinese with English abstract).
- Eizenhöfer, P. R., Zhao, G., Zhang, J., et al., 2014. Final Closure of the Paleo-Asian Ocean along the Solonker Suture Zone: Constraints from Geochronological and Geochemical Data of Permian Volcanic and Sedimentary Rocks. *Tectonics*, 33 (4): 441—463. doi: 10.1002/2013TC003357
- Eizenhöfer, P. R., Zhao, G. C., Zhang, J., et al., 2015. Geochemical Characteristics of the Permian Basins and Their Provenances across the Solonker Suture Zone: Assessment of Net Crustal Growth during the Closure of the Palaeo-Asian Ocean. *Lithos*, 224—225: 240—255. doi: 10.1016/j.lithos.2015.03.012
- Elliott, T., Plank, T., Zindler, A., et al., 1997. Element Transport from Slab to Volcanic Front at the Mariana Arc. *Journal of Geophysical Research Solid Earth*, 102 (B7): 14991—15019. doi: 10.1029/97JB00788
- Frost, B. R., Barnes, C. G., Collins, W. J., et al., 2001. A Geochemical Classification for Granitic Rocks. *Journal of Petrology*, 42(11): 2033—2048.
- Frost, C. D., Frost, B. R., Chamberlain, K. R., et al., 1999. Petrogenesis of the 1.43 Ga Sherman Batholith, SE Wyoming, USA: A Reduced, Rapakivi-Type Anorogenic Granite. *Journal of Petrology*, 40(12). doi: 10.1093/petroj/40.12.1771
- Griffin, W. L., Pearson, N. J., Belousova, E., et al., 2000. The Hf Isotope Composition of Cratonic Mantle: LAM-MC-ICPMS Analysis of Zircon Megacrysts in Kimberlites. *Geochimica et Cosmochimica Acta*, 64(1): 133—147. doi: 10.1016/S0016-7037(99)00343-9
- Griffin, W. L., Wang, X., Jackson, S. E., et al., 2002. Zircon Chemistry and Magma Mixing, SE China: In-situ Analysis of Hf Isotopes, Tonglu and Pingtan Igneous Complexes. *Lithos*, 61(3): 237—269. doi: 10.1016/S0024-4937(02)00082-8
- Han, B. F., Wang, S. G., Jahn, B. M., et al., 1997. Depleted-mantle Source for the Ulungur River A-type Granites from North Xinjiang, China; Geochemistry and Nd-Sr Isotopic Evidence, and Implications for Phanerozoic Crustal Growth. *Annals of Thoracic Surgery*, 138(3—4): 135—159. doi: 10.1016/S0009-2541(97)00003-X
- Han, G. Q., Liu, Y. J., Neubauer, F., et al., 2012. Provenance Analysis of Permian Sandstones in the Central and Southern Da Xing'an Mountains, China: Constraints on the Evolution of the Eastern Segment of the Central Asian Orogenic Belt. *Tectonophysics*, 580 (2): 100—113. doi: 10.1016/j.tecto.2012.08.041
- Han, J., Zhou, J. B., Wang, B., et al., 2015. The Final Collision of the CAOB: Constraint from the Zircon U-Pb Dating of the Linxi Formation, Inner Mongolia. *Geoscience Frontiers*, 6 (2): 211—225. doi: 10.1016/j.gsf.2014.06.003
- Hawkesworth, C. J., Turner, S. P., McDermott, F., et al., 1997. U-Th Isotopes in Arc Magmas: Implications for Element Transfer from the Subducted Crust. *Science*, 276 (5312): 551—555. doi: 10.1126/science.276.5312.551
- Hirose, K., 1997. Melting Experiments on Lherzolite KLBl under Hydrous Conditions and Generation of High-magnesian Andesitic Melts. *Geology*, 25 (1): 42—44.
- Elliott, T., 2013. Tracers of the Slab. Inside the Subduction Factory. *American Geophysical Union*.

- doi:10.1130/0091-7613(1997)025<0042:MEOLKU>2.3.CO;2
- Hong, D. W. , Huang, H. Z. , Xiao, Y. J. , et al. , 1995. Permian Alkaline Granites in Central Inner Mongolia and Their Geodynamic Significance. *Acta Geologica Sinica*, 81(1): 27—39. doi: 10. 1111/j. 1755 — 6724. 1995. mp8001003. x
- Hoskin, P. W. O. , Black, L. P. , 2000. Metamorphic Zircon Formation by Solid-State Recrystallization of Protolith Igneous Zircon. *Journal of Metamorphic Geology*, 18(4): 423—439. doi: 10. 1046/j. 1525 — 1314. 2000. 00266. x
- Hu, C. S. , Li, W. B. , Xu, C. , et al. , 2015. Geochemistry and Zircon U-Pb-Hf Isotopes of the Granitoids of Baolidao and Halatu Plutons in Sonidzuoqi Area, Inner Mongolia: Implications for Petrogenesis and Geodynamic Setting. *Journal of Asian Earth Sciences*, 97: 294—306. doi:10.1016/j.jseas.2014.07.030
- Irvine, T. N. , Baragar, W. R. A. , 1971. A Guide to the Chemical Classification of the Common Volcanic Rocks. *Canadian Journal of Earth Sciences*, 8(5):523—548.
- Jahn, B. M. , Capdevila, R. , Liu, D. , et al. , 2004a. Sources of Phanerozoic Granitoids in the Transect Bayanhongor-Ulaan Baatar, Mongolia: Geochemical and Nd Isotopic Evidence, and Implications for Phanerozoic Crustal Growth. *Journal of Asian Earth Sciences*, 23(5): 629—653.
- Jahn, B. M. , Windley, B. , Natal'in, B. , et al. 2004b. Phanerozoic Continental Growth in Central Asia. *Journal of Asian Earth Sciences*, 23(5): 599—603. doi: 10. 1016/S1367-9120(03)00124-X
- Jian, P. , Liu, D. Y. , Kröner, A. , et al. , 2008. Time Scale of An Early to Mid-Paleozoic Orogenic Cycle of the Long-lived Central Asian Orogenic Belt, Inner Mongolia of China: Implications for Continental Growth. *Lithos*, 101(3):233—259. doi:10.1016/j.lithos.2007.07.005
- Jian, P. , Liu, D. Y. , Kröner, A. , et al. , 2010. Evolution of a Permian Intraoceanic Arc-Trench System in the Solonker Suture Zone, Central Asian Orogenic Belt, China and Mongolia. *Lithos*, 118(118): 169—190. doi: 10. 1016/j.lithos.2010.04.014
- Kang, J. L. , Xiao, Z. B. , Wang, H. C. , et al. , 2016. Late Paleozoic Subduction of the Paleo-Asian Ocean: Geochronological and Geochemical Evidence from the Meta-basic Volcanics of Xilinhhot, Innet Mongolia. *Acta Geologica Sinica*, 02(90):383—397 (in Chinese with English abstract).
- Kelemen, P. B. , Hanghoj, K. , Greene, A. R. , 2007. One View of the Geochemistry of Subduction-Related Magmatic Arcs, with an Emphasis on Primitive Andesite and Lower Crust. *Treatise on Geochemistry*, 138:1—70.
- Kovalenko, V. I. , Yarmolyuk, V. V. , Kovach, V. P. , et al. , 2004. Isotope Provinces, Mechanisms of Generation and Sources of the Continental Crust in the Central Asian Mobile Belt: Geological and Isotopic Evidence. *Journal of Asian Earth Sciences*, 23(5):605—627.
- Kröner, A. , Kovach, V. , Belousova, E. , et al. , 2014. Reassessment of Continental Growth during the Accretionary History of the Central Asian Orogenic Belt. *Gondwana Research*, 25(1):103—125.
- Le Maitre, R. W. , 2002. Igneous Rocks, A Classification and Glossary of Terms. *Cambridge University Press, Cambridge*, (2nd ed.):1—193.
- Li, B. X. , 2014. Research on Disintegration and Chronology of Xilin Gol Complex in Xiwuqi, Inner Mongolia (Dissertation). China University of Geosciences, Beijing, 57—63 (in Chinese with English abstract).
- Li, D. P. , Jin, Y. , Hou, K. J. , et al. , 2015a. Late Paleozoic Final Closure of the Paleo-Asian Ocean in the Eastern Part of the Xing-Meng Orogenic Belt: Constraints from Carboniferous-Permian (Meta-) Sedimentary Strata and (Meta-) Igneous Rocks. *Tectonophysics*, 665: 251—262. doi:10.1016/j.tecto.2015.10.007
- Li, J. Y. , 1998. Some New Ideas on Tectonics of NE China and Its Neighboring Areas. *Geological Review*, 44(4): 339—347 (in Chinese with English abstract).
- Li, J. Y. , 2006. Permian Geodynamic Setting of Northeast China and Adjacent Regions: Closure of the Paleo-Asian Ocean and Subduction of the Paleo-Pacific Plate. *Journal of Asian Earth Sciences*, 26(3):207—224. doi:10. 1016/j.jseas.2005.09.001
- Li, J. Y. , Guo, F. , Li, C. W. , et al. , 2015b. Permian Back-Arc Extension in Central Inner Mongolia, NE China: Elemental and Sr-Nd-Pb-Hf-O Isotopic Constraints from the Linxi high-MgO Diabase Dikes. *Island Arc*, 24(4): 404—424. doi:10.1111/iar.12120
- Li, J. Y. , Zhang, J. , Yang, T. N. , et al. , 2009. Crustal Tectonic Division and Evolution of the Southern Part of the North Asian Orogenic Region and Its Adjacent Areas. *Journal of Jinlin University (Earth Science Edition)*, 39(4):584—605 (in Chinese with English abstract).
- Li, R. J. , 2013. The Research of Geochemical Characteristics, Geochronology and Geological Significance of The Benbatu Formation Volcanic Rocks of The Xiwuqi Area in Inner Mongolia (Dissertation). China University of Geosciences, Beijing, 48—51 (in Chinese with English abstract).

- abstract).
- Li, S., Wilde, S. A., He, Z. J., et al., 2002. Triassic Sedimentation and Postaccretionary Crustal Evolution along the Solonker Suture Zone in Inner Mongolia, China. *Acp Journal Club*, 137 (6): 192. doi: 10.1002/2013TC003444
- Li, S., Wilde, S. A., Wang, T., et al., 2016a. Latest Early Permian Granitic Magmatism in Southern Inner Mongolia, China: Implications for the Tectonic Evolution of the Southeastern Central Asian Orogenic Belt. *Gondwana Research*, 19 (1): 168—180. doi: 10.1016/j.gr.2014.11.006
- Li, Y. L., Brouwer, F. M., Xiao, W. J., et al., 2016b. Subduction-related Metasomatic Mantle Source in the Eastern Central Asian Orogenic Belt: Evidence from Amphibolites in the Xilingol Complex, Inner Mongolia, China. *Gondwana Research*, 43: 193—212. doi: 10.1016/j.gr.2015.11.015
- Li, Y. L., Zhou, H. W., Brouwer, F. M., et al., 2011. Tectonic Significance of the Xilin Gol Complex, Inner Mongolia, China: Petrological, Geochemical and U-Pb Zircon Age Constraints. *Journal of Asian Earth Sciences*, 42 (5): 1018—1029. doi: 10.1016/j.jseaes.2010.09.009
- Li, Y. L., Zhou, H. W., Brouwer, F. M., et al., 2014. Nature and Timing of the Solonker Suture of the Central Asian Orogenic Belt: Insights from Geochronology and Geochemistry of Basic Intrusions in the Xilin Gol Complex, Inner Mongolia, China. *International Journal of Earth Sciences*, 103(1): 41—60. doi: 10.1007/s00531-013-0931-3
- Li, Y. L., Zhou, H. W., Xiao, W. J., et al., 2012. Superposition of Paleo-Asian and West-Pacific Tectonic Domains in the Eastern Section of the Solonker Suture Zone: Insights from Petrology, Geochemistry and Geochronology of Deformed Diorite in Xar Moron Fault Zone, Inner Mongolia. *Earth Science*, 37(3): 432—450 (in Chinese with English abstract).
- Liu, J. F., 2009. Late Paleozoic Magmatism and Its Constraints on Regional Tectonic Evolution in Linxi-Dongwuqi Area, Inner Mongolia (Dissertation). Jilin University, Changchun, 67—112 (in Chinese with English abstract).
- Liu, J. F., Chi, X. G., Zhang, X. Z., et al., 2009. Geochemical Characteristic of Carboniferous Quartz-Diorite in the Southern Xiwuqi Area, Inner Mongolia and Its Tectonic Significance. *Acta Geologica Sinica*, 83(3): 365—376 (in Chinese with English abstract).
- Liu, J. F., Chi, X. G., Zhao, Z., et al., 2011. Geochemical Characteristics and Geological Significance of Early Permian Baya'ertuhushuo Gabbro in South Great Xing'an Range. *Acta Geologica Sinica*, 85(1): 116—129. doi: 10.1111/j.1755-6724.2011.00384.x
- Liu, J. F., Jiang, S. H., Zhang, Y., 2010. The SHRIMP Zircon U-Pb Dating and Geochemical Features of Bairendaba Diorite in the Xilinhaote Area, Inner Mongolia, China. *Geological Bulletin of China*, 29(5): 688—696 (in Chinese with English abstract).
- Liu, J. F., Li, J. Y., Chi, X. G., et al., 2013. A Late-Carboniferous to Early Early-Permian Subduction-Accretion Complex in Daqing Pasture, Southeastern Inner Mongolia; Evidence of Northward Subduction Beneath the Siberian Paleoplate Southern Margin. *Lithos*, 177(2): 285—296. doi: 10.1016/j.lithos.2013.07.008
- Liu, W., Pan, X. F., Liu, D. Y., et al., 2009. Three-Step Continental-Crust Growth from Subduction Accretion and Underplating, through Intermediary Differentiation, to Granitoid Production. *International Journal of Earth Sciences*, 98 (6): 1413—1439. doi: 10.1007/s00531-008-0299-y
- Liu, Y. S., Gao, S., Hu, Z. C., et al., 2010. Continental and Oceanic Crust Recycling-Induced Melt-Peridotite Interactions in the Trans-North China Orogen: U-Pb Dating, Hf Isotopes and Trace Elements in Zircons from Mantle Xenoliths. *Journal of Petrology*, 51(1—2): 537—571. doi: 10.1093/petrology/egp082
- Liu, Y. S., Hu, Z. C., Gao, S., et al., 2008. In Situ Analysis of Major and Trace Elements of Anhydrous Minerals by LA-ICP-MS without Applying an Internal Standard. *Chemical Geology*, 257(1—2): 34—43. doi: 10.1016/j.chemgeo.2008.08.004
- Ludwig, K. R., 2003. ISOPLOT, A Geochronological Toolkit for Microsoft Excel 3.00. Berkeley Geochronology Center, Berkeley.
- Mahoney, J. J., Coffin, M. F., 2013. Plume/Lithosphere Interaction in the Generation of Continental and Oceanic Flood Basalts; Chemical and Isotopic Constraints. Large Igneous Provinces: Continental, Oceanic, and Planetary Flood Volcanism. American Geophysical Union, Washington.
- Miao, L. C., Fan, W. M., Liu, D. Y., et al., 2008. Geochronology and Geochemistry of the Hegenshan Ophiolitic Complex: Implications for Late-Stage Tectonic Evolution of the Inner Mongolia-Daxinganling Orogenic Belt, China. *Journal of Asian Earth Sciences*, 32 (5—6): 348—370. doi: 10.1016/j.jseaes.2007.11.005
- Middlemost, E. A. K., 1994. Naming Materials in the Mag-

- ma/Igneous Rock System. *Earth Science Reviews*, 37(3—4):215—224. doi:10.1016/0012—8252(94)90029—9
- Pan, S. Y., Chi, X. G., Sun, W., et al., 2012. Geochemical Characteristics and Tectonic Significance of Late Carboniferous Volcanic Rocks in Benbatu Formation of Sonid Youqi, Inner Mongolia. *Global Geology*, 31(1): 40—50 (in Chinese with English abstract).
- Pearce, J. A., 2008. Geochemical Fingerprinting of Oceanic Basalts with Applications to Ophiolite Classification and the Search for Archean Oceanic Crust. *Lithos*, 100(1—4):14—48. doi:10.1016/j.lithos.2007.06.016
- Peccerillo, A., Taylor, S. R., 1976. Geochemistry of Eocene Calc-Alkaline Volcanic Rocks from the Kastamonu Area, Northern Turkey. *Contributions to Mineralogy & Petrology*, 58(1):63—81. doi:10.1007/BF00384745
- Pin, C., Paquette, J. L., 1997. A Mantle-Derived Bimodal Suite in the Hercynian Belt: Nd Isotope and Trace Element Evidence for a Subduction-related Rift Origin of the Late Devonian Brévenne Metavolcanics, Massif Central (France). *Contributions to Mineralogy & Petrology*, 129(129):222—238. doi:10.1007/s004100050334
- Rickwood, P. C., 1989. Boundary Lines within Petrologic Diagrams Which Use Oxides of Major and Minor Elements. *Lithos*, 22(4):247—263. doi:10.1016/0024—4937(89)90028—5
- Saunders, A. D., Storey, M., Kent, R. W., et al., 1992. Consequences of Plume-Lithosphere Interactions. *Geological Society London Special Publications*, 68(1):41—60. doi:10.1144/GSL.SP.1992.068.01.04
- Sengör, A. M. C., Natal'in, B. A., Burtman, V. S., 1993. Evolution of the Altai Tectonic Collage and Paleozoic Crustal Growth in Eurasia. *Nature*, 364:299—307. doi:10.1038/364299a0
- Shao, J. A., Mou, B. L., He, G. Q., et al., 1997. Geological Process of Northern North China during the Structural Superimposition between Paleo-Asian Oceanic Tectonic Domain and Paleo-Pacific Oceanic Tectonic Domain. *Science in China (Series D)*, 27(5):390—394 (in Chinese).
- Shi, G. H., Miao, L. C., Zhang, F. Q., et al., 2004. Emplacement Age and Tectonic Implications of the Xilinhhot A-type Granite in Inner Mongolia, China. *Chinese Science Bulletin*, 49(7):723—729. doi:10.1007/BF03184272
- Shi, Y. R., Jian, P., Kröner, A., et al., 2016. Zircon Ages and Hf Isotopic Compositions of Ordovician and Carboniferous Granitoids from Central Inner Mongolia and their Significance for Early and Late Paleozoic Evolution of the Central Asian Orogenic Belt. *Journal of Asian Earth Sciences*, 117(3):153—169. doi:10.1016/j.jseae.2015.12.007
- Shi, Y. R., Liu, C., Deng, J. F., et al., 2014. Geochronological Frame of Granitoids from Central Inner Mongolia and Its Tectono-magmatic Evolution. *Acta Petrologica Sinica*, 30(11):3155—3171 (in Chinese with English abstract).
- Shimoda, G., Tatsumi, Y., Nohda, S., et al., 1998. Setouchi High-Mg Andesites Revisited: Geochemical Evidence for Melting of Subducting Sediments. *Earth & Planetary Science Letters*, 160(3):479—492. doi:10.1016/S0012—821X(98)00105—8
- Sun, S. S., McDonough, W. F., 1989. Chemical and Isotopic Systematics of Oceanic Basalts; Implications for Mantle Composition and Processes. *Geological Society London Special Publications*, 42(1):313—345. doi:10.1144/GSL.SP.1989.042.01.19
- Söderlund, U., Patchett, P. J., Vervoort, J. D., et al., 2004. The ¹⁷⁶Lu Decay Constant Determined by Lu-Hf and U-Pb Isotope Systematics of Precambrian Mafic Intrusions. *Earth & Planetary Science Letters*, 219(3—4): 311—324. doi:10.1016/S0012—821X(04)00012—3
- Tang, G. J., Wang, Q., 2010. High-Mg Andesites and their Geodynamic Implications. *Acta Petrologica Sinica*, 26(8):2495—2512 (in Chinese with English abstract).
- Tang, K. D., 2002. Tectonic Development of Paleozoic Fold-belts at the North Margin of the Sino-Korean Craton. *Plant Growth Regulation*, 36(3):241—244. doi:10.1029/TC009j002p00249
- Tong, Y., Jahn, B. M., Wang, T., et al., 2015. Permian Alkaline Granites in the Erenhot-Hegenshan Belt, Northern Inner Mongolia, China: Model of Generation, Time of Emplacement and Regional Tectonic Significance. *Journal of Asian Earth Sciences*, 97 (Part B): 320—336. doi:10.1016/j.jseae.2014.10.011
- Vervoort, J. D., Patchett, P. J., Gehrels, G. E., et al., 1996. Constraints on Early Earth Differentiation from Hafnium and Neodymium Isotopes. *Nature*, 379 (6566): 624—627. doi:10.1038/379624a0
- Wang, J., Sun, F. Y., Li, B. L., et al., 2016. Age, Petrogenesis and Tectonic Implications of Permian Hornblende in Tugurige, Urad Zhongqi, Inner Mongolia. *Earth Science*, 41(5):792—808 (in Chinese with English abstract).
- Wang, S. Q., Xin, H. T., Hu, X. J., et al., 2016. Geochronology, Geochemistry and Geological Significance of Early Paleozoic Wulanaobaotu Intrusive Rocks, Inner Mongolia. *Earth Science*, 41(4):555—569 (in Chinese with English abstract).

- English abstract).
- Wilde, S. A., 2015. Final Amalgamation of the Central Asian Orogenic Belt in NE China: Paleo-Asian Ocean Closure versus Paleo-Pacific Plate Subduction—A Review of the Evidence. *Tectonophysics*, 662(1): 345—362. doi: 10.1016/j.tecto.2015.05.006
- Wilhem, C., Windley, B. F., Stampfli, G. M., 2012. The Altaiids of Central Asia: A Tectonic and Evolutionary Innovative Review. *Earth-Science Reviews*, 113 (113): 303—341. doi: 10.1016/j.earscirev.2012.04.001
- Windley, B. F., Alexeiev, D., Xiao, W., et al., 2007. Tectonic Models for Accretion of the Central Asian Orogenic Belt. *Journal of the Geological Society*, 164(1): 31—47. doi: 10.1144/0016-76492006-022
- Wu, F. Y., Yang, Y. H., Xie, L. W., et al., 2006. Hf Isotopic Compositions of the Standard Zircons and Baddeleyites Used in U-Pb Geochronology. *Chemical Geology*, 234: 105—126. doi: 10.1016/j.chemgeo.2006.05.003
- Wu, F. Y., Zhao, G. C., Sun, D. Y., et al., 2007. The Hulan Group: Its Role in the Evolution of the Central Asian Orogenic Belt of NE China. *Journal of Asian Earth Sciences*, 30(3—4): 542—556. doi: 10.1016/j.jseas.2007.01.003
- Xiao, W. J., Windley, B. F., Hao, J., et al., 2003. Accretion Leading to Collision and the Permian Solonker Suture, Inner Mongolia, China: Termination of the Central Asian Orogenic Belt. *Tectonics*, 22(6): 8—20. doi: 10.1029/2002TC001484
- Xiao, W. J., Windley, B. F., Huang, B. C., et al., 2009. End-Permian to Mid-Triassic Termination of the Accretionary Processes of the Southern Altaiids; Implications for the Geodynamic Evolution, Phanerozoic Continental Growth, and Metallogeny of Central Asia. *International Journal of Earth Sciences*, 98(6): 1189—1217. doi: 10.1007/s00531-008-0407-z
- Xiao, W. J., Windley, B. F., Sun, S., et al., 2015. A Tale of Amalgamation of Three Permo-Triassic Collage Systems in Central Asia: Oroclines, Sutures, and Terminal Accretion. *Annual Review of Earth & Planetary Sciences*, 43: 477—507. doi: 10.1146/annurev-earth-060614-105254
- Xiao, W. J., Zhang, L. C., Qin, K. Z., et al., 2004. Paleozoic Accretionary and Collisional Tectonics of the Eastern Tianshan (China): Implications for the Continental Growth of Central Asia. *American Journal of Science*, 304: 370—395. doi: 10.2475/ajs.304.4.370
- Xu, B., Charvet, J., Chen, Y., et al., 2013a. Middle Paleozoic Convergent Orogenic Belts in Western Inner Mongolia (China): Framework, Kinematics, Geochronology and Implications for Tectonic Evolution of the Central Asian Orogenic Belt. *Gondwana Research*, 23 (4): 1342—1364. doi: 10.1016/j.gr.2012.05.015
- Xu, W. L., Pei, F. P., Wang, F., et al., 2013b. Spatial-temporal Relationships of Mesozoic Volcanic Rocks in NE China: Constraints on Tectonic Overprinting and Transformations between Multiple Tectonic Regimes. *Journal of Asian Earth Sciences*, 74 (18): 167—193. doi: 10.1016/j.jseas.2013.04.003
- Xue, H. M., Guo, L. J., Hou, Z. Q., et al., 2009. The Xilin-gele Complex from the Eastern Part of the Central Asian-Mongolia Orogenic Belt, China: Products of Early Variscan Orogeny Other than Ancient Block: Evidence from Zircon SHRIMP U-Pb Ages. *Acta Petrologica Sinica*, 25(8): 2001—2010 (in Chinese with English abstract).
- Yang, J. H., Wu, F. Y., Shao, J. A., et al., 2006. Constraints on the Timing of Uplift of the Yanshan Fold and Thrust Belt, North China. *Earth & Planetary Science Letters*, 246 (3—4): 336—352. doi: 10.1016/j.epsl.2006.04.029
- Yuan, H. L., Gao, S., Dai, M. N., et al., 2008. Simultaneous Determinations of U-Pb Age, Hf Isotopes and Trace Element Compositions of Zircon by Excimer Laser-Ablation Quadrupole and Multiple-Collector ICP-MS. *Chemical Geology*, 247(1—2): 100—118. doi: 10.1016/j.chemgeo.2007.10.003
- Zhang, S. H., Gao, R., Li, H. Y., et al., 2014a. Crustal Structures Revealed from a Deep Seismic Reflection Profile across the Solonker Suture Zone of the Central Asian Orogenic Belt, Northern China: An Integrated Interpretation. *Tectonophysics*, 612—613: 26—39. doi: 10.1016/j.tecto.2013.11.035
- Zhang, S. H., Zhao, Y., Kröner, A., et al., 2008a. Early Permian Plutons from the Northern North China Block: Constraints on Continental Arc Evolution and Convergent Margin Magmatism Related to the Central Asian Orogenic Belt. *International Journal of Earth Sciences*, 98(6): 1441—1467. doi: 10.1007/s00531-008-0368-2
- Zhang, S. H., Zhao, Y., Song, B., et al., 2007. Carboniferous Granitic Plutons from the Northern Margin of the North China Block: Implications for a Late Paleozoic Active Continental Margin. *Journal of the Geological Society*, 164 (2): 451—463. doi: 10.1144/0016-76492005-190
- Zhang, S. H., Zhao, Y., Song, B., et al., 2009. Contrasting

- Late Carboniferous and Late Permian-Middle Triassic Intrusive Suites from the Northern Margin of the North China Craton: Geochronology, Petrogenesis, and Tectonic Implications. *Geological Society of America Bulletin*, 121(121): 181—200. doi:10.1130/B26157.1
- Zhang, X. H., Wilde, S. A., Zhang, H. F., 2011. Early Permian high-K Calc-Alkaline Volcanic Rocks from NW Inner Mongolia, North China: Geochemistry, Origin and Tectonic Implications. *Journal of the Geological Society*, 168 (2): 525—543. doi:10.1144/0016-76492010-094
- Zhang, X. H., Zhai, M. G., 2010. Magmatism and Its Metallogenetic Effects during the Paleozoic Continental Crustal Construction in Northern North China: An Overview. *Acta Petrologica Sinica*, 26 (5): 1329—1341 (in Chinese with English abstract).
- Zhang, X. H., Zhang, H. F., Tang, Y. J., et al., 2008b. Geochemistry of Permian Bimodal Volcanic Rocks from Central Inner Mongolia, North China: Implication for Tectonic Setting and Phanerozoic Continental Growth in Central Asian Orogenic Belt. *Chemical Geology*, 249 (3): 262—281. doi:10.1016/j.chemgeo.2008.01.005
- Zhang, Z., Zhang, H. F., Shao, J. A., et al., 2014b. Mantle Upwelling during Permian to Triassic in the Northern Margin of the North China Craton: Constraints from Southern Inner Mongolia. *Journal of Asian Earth Sciences*, 79 (2): 112—129. doi: 10.1016/j.jseaes.2013.09.015
- Zheng, Y. F., Zhang, S. B., Zhao, Z. F., et al., 2007. Contrasting Zircon Hf and O Isotopes in the Two Episodes of Neoproterozoic Granitoids in South China: Implications for Growth and Reworking of Continental Crust. *Lithos*, 96 (1—2): 127—150. doi: 10.1016/j.lithos.2006.10.003
- Zhou, J. B., Wilde, S. A., 2013. The Crustal Accretion History and Tectonic Evolution of the NE China Segment of the Central Asian Orogenic Belt. *Gondwana Research*, 23(4): 1365—1377. doi:10.1016/j.gr.2012.05.012
- Zhou, J. B., Wilde, S. A., Zhang, X. Z., et al., 2011. Early Paleozoic Metamorphic Rocks of the Erguna Block in the Great Xing'an Range, NE China: Evidence for the Timing of Magmatic and Metamorphic Events and their Tectonic Implications. *Tectonophysics*, 499 (1—4): 105—117. doi:10.1016/j.tecto.2010.12.009
- Zhou, W. X., 2012. Studied of Geochronology and Geochemistry of Paleozoic Magmatism in Xilinhot Area, Inner Mongolia (Dissertation). China University of Geosciences, Wuhan, 35—96 (in Chinese with English abstract).
- Zhou, W. X., Ge, M. C., 2013. Redefinition and Significance of Metamorphism Xilinhot Group in Xilinhot Area, Inner Mongolia, China. *Earth Science*, 38(4): 715—724 (in Chinese with English abstract).
- Zhou, Z. G., Gu, Y. C., Liu, C. F., et al., 2010. Discovery of Early-Middle Permian Cathaysian Flora in Manduhubaolage Area, Dong Ujimqin Qi, Inner Mongolia, China and Its Geological Significance. *Geological Bulletin of China*, 29 (1): 21—25 (in Chinese with English abstract).
- ### 附中文参考文献
- 鲍庆中,张长捷,吴之理,等,2007.内蒙古白音高勒地区石炭纪石英闪长岩 SHRIMP 锆石 U-Pb 年代学及其意义. 吉林大学学报:地球科学版,37(1): 15—23.
- 陈斌,马星华,刘安坤,等,2009.锡林浩特杂岩和蓝片岩的锆石 U-Pb 年代学及其对索伦缝合带演化的意义. 岩石学报,25(12): 3123—3129.
- 晨辰,张志诚,郭召杰,等,2012.内蒙古达茂旗满都拉地区早二叠世基性岩的年代学、地球化学及其地质意义. 地球科学,42(3): 343—358.
- 陈彦,张志诚,李可,等,2014.内蒙古西乌旗地区二叠纪双峰式火山岩的年代学、地球化学特征和地质意义. 北京大学学报:自然科学版,50(5): 843—858.
- 邓晋福,刘翠,冯艳芳,等,2010.高镁安山岩/闪长岩类(HMA)和镁安山岩/闪长岩类(MA):与洋俯冲作用相关的两类典型的火成岩类. 中国地质, 37 (4): 1112—1118.
- 邓晋福,冯艳芳,狄永军,等,2015.岩浆弧火成岩构造组合与洋陆转换. 地质论评,61(3): 473—484.
- 康健丽,肖志斌,王惠初,等,2016.内蒙古锡林浩特早石炭世构造环境:来自变质基性火山岩的年代学和地球化学证据. 地质学报,2(90): 383—397.
- 李宝霞,2014.内蒙古西乌旗锡林郭勒杂岩的解体与年代学研究(硕士学位论文).北京:中国地质大学,57—63.
- 李锦铁,1998.中国东北及邻区若干地质构造问题的新认识. 地质论评,44(4): 339—347.
- 李锦铁,张进,杨天南,等,2009.北亚造山区南部及其毗邻地区地壳构造分区与构造演化. 吉林大学学报(地球科学版),39(4): 584—605.
- 李瑞杰,2013.内蒙古西乌旗本巴图组火山岩地球化学特征、年代学及地质意义研究(硕士学位论文).北京:中国地质大学,48—51.
- 李益龙,周汉文,肖文交,等,2012.古亚洲构造域和西太平洋构造域在索伦缝合带东段的叠加:来自内蒙古西县西拉木伦断裂带内变形闪长岩的岩石学、地球化学和年代学证据. 地球科学,37(3): 433—450.
- 刘建峰,2009.内蒙古林西—东乌旗地区晚古生代岩浆作用

- 及其对区域构造演化的制约(博士学位论文). 长春: 吉林大学, 67—112.
- 刘建峰, 迟效国, 张兴洲, 等, 2009. 内蒙古西乌旗南部石炭纪石英闪长岩地球化学特征及其构造意义. 地质学报, 83(3): 365—376.
- 刘翼飞, 江思宏, 张义, 2010. 内蒙古锡林浩特地区拜仁达坝矿区闪长岩体锆石 SHRIMP U-Pb 定年及其地质意义. 地质通报, 29(5): 688—696.
- 潘世语, 迟效国, 孙巍, 等, 2012. 内蒙古苏尼特右旗晚石炭世本巴图组火山岩地球化学特征及构造意义. 世界地质, 31(1): 40—50.
- 邵济安, 卞保磊, 何国琦, 等, 1997. 华北北部在古亚洲域与古太平洋域构造叠加过程中的地质作用. 中国科学(D辑), 27(5): 390—394.
- 石玉若, 刘翠, 邓晋福, 等, 2014. 内蒙古中部花岗质岩类年代学格架及该区构造岩浆演化探讨. 岩石学报, 30(11): 3155—3171.
- 唐功建, 王强, 2010. 高镁安山岩及其地球动力学意义. 岩石学报, 26(8): 2495—2512.
- 王键, 孙丰月, 李碧乐, 等, 2016. 内蒙乌拉特中旗图古日格二叠纪角闪石岩年龄、岩石成因及构造背景. 地球科学, 41(5): 792—808.
- 王树庆, 辛后田, 胡晓佳, 等, 2016. 内蒙古乌兰敖包图早古生代侵入岩年代学、地球化学特征及地质意义. 地球科学, 41(4): 555—569.
- 薛怀民, 郭利军, 侯增谦, 等, 2009. 中亚—蒙古造山带东段的锡林郭勒杂岩: 早华力西期造山作用的产物而非古老陆块? —锆石 SHRIMP U-Pb 年代学证据. 岩石学报, 25(8): 2001—2010.
- 张晓晖, 翟明国, 2010. 华北北部古生代大陆地壳增生过程中的岩浆作用与成矿效应. 岩石学报, 26(5): 1329—1341.
- 周文孝, 2012. 内蒙古锡林浩特地区古生代岩浆作用的年代学与地球化学研究(博士学位论文). 武汉: 中国地质大学, 35—96.
- 周文孝, 葛梦春, 2013. 内蒙古锡林浩特地区中元古代锡林浩特岩群的厘定及其意义. 地球科学, 38(4): 715—724.
- 周志广, 谷永昌, 柳长峰, 等, 2010. 内蒙古东乌珠穆沁旗满都胡宝拉格地区早—中二叠世华夏植物群的发现及地质意义. 地质通报, 29(1): 21—25.